MULTIPERIOD OPTIMAL POWER FLOW PROBLEM IN DISTRIBUTION SYSTEM PLANNING

by

Jaap Pedersen

5132635

Master's thesis in Computational Sciences

at

Department of Mathematics and Computer Science,

Free University of Berlin

Supervisor: Prof. Dr. Ralf Borndörfer

In cooperation with

Reiner-Lemoine Institute, Berlin

December 2019

Abstract

Growing demand, distributed generation, such as renewable energy sources (RES), and the increasing role of storage systems to mitigate the volatility of RES on a medium voltage level, push existing distribution grids to their limits. Therefore, necessary network expansion needs to be evaluated to guarantee a safe and reliable electricity supply in the future taking these challenges into account.

This problem is formulated as an optimal power flow (OPF) problem which combines network expansion, volatile generation and storage systems, minimizing network expansion and generation costs. As storage systems introduce a temporal coupling into the system, a multiperiod OPF problem is needed and analysed in this thesis.

To reduce complexity, the network expansion problem is represented in a continuous nonlinear programming formulation by using fundamental properties of electrical engeneering. This formulation is validated succesfully against a common mixed integer programming approach on a 30 and 57 bus network with respect to solution and computing time.

As the OPF problem is, in general, a nonconvex, nonlinear problem and, thus, hard to solve, convex relaxations of the power flow equations have gained increasing interest. Sufficient conditions are represented which guarantee exactness of a second-order cone (SOC) relaxation of an operational OPF in radial networks. In this thesis, these conditions are enhanced for the network expansion planning problem. Additionally, nonconvexities introduced by the choice of network expansion variables are relaxed by using McCormick envelopes.

These relaxations are then applied on the multiperiod OPF and compared to the original problem on a 30 and a 57 bus network. In particular, the computational time is decreased by an order up to 10^2 by the SOC relaxation while it provides either an exact solution or a sufficient lower bound on the original problem. Finally, a sensitivity study is performed on weights of network expansion costs showing strong dependency of both the solution of performed expansion and solution time on the chosen weights.

Contents

List of Figures

List of Tables

List of Abbreviations

BFM	Branch Flow Model
BIM	Bus Injection Model
DG	Distributed Generation
IEEE	Institute of Electrical and Electronics Engineers
MINLP	Mixed Integer Nonlinear Programming
MIP	Mixed Integer Programming
MPLM	Multiple Parallel Line Model
MPLP	Multiple Parallel Line Programming
NEP	Network Expansion Planning
NLP	Nonlinear Programming
OPF	Optimal Power Flow
RES	Renewable Energy Sources
SDP	Semidefinite Programming
SOC	Second-Order Cone
SOCP	Second-Order Cone Programming

List of Symbols

General

G	graph $G = (N, E)$ representing a network
N	set of nodes in a network, $N = \{0, 1, \ldots, n\}$
E	set of edges in a network
S	set of storage nodes in a network
(i, j), ij	line from node i to node j
$\mathcal{T}$	time horizon with t timesteps of length $\mathbf{T_s}$
$\mathbf{T_s}$	length of time step
$\boldsymbol{j}$	imaginary unit
A^*	complex conjugate of a complex variable A

Variables

s_i	apparent power injection at bus i, $s_i = p_i + \boldsymbol{j} q_i$
p_i, q_i	active and reactive power injection at bus i, $p_i = p_i^g + \mathbf{p_i^c}$, $q_i = q_i^g + \mathbf{q_i^c}$
p_i^g, q_i^g	active and reactive power output of generator at bus i
v_i	squared voltage magnitude at bus i
S_{ik}	apparent power flow over line ik, $S_{ik} = P_{ik} + \boldsymbol{j} Q_{ik}$
P_{ik}, Q_{ik}	active and reactive power flow over line ik
ℓ_{ik}	squared current magnitude over line ik
I_{ik}^{max}	maximal allowed current flow over line ik
z_{ik}	impedance of line ik, $z_{ik} = r_{ik} + \boldsymbol{j} x_{ik}$
r_{ik}, x_{ik}	resistance and reactance of line ik
$u_{c,i}$,$u_{d,i}$	charging and discharging rate of storage at bus i
e_i^t, e_i^{t+1}	state of charge of storage at bus i at time t and time $t+1$

Parameter

$\mathbf{p_i^c}$, $\mathbf{q_i^c}$	active and reactive power demand at bus i
$\mathbf{g_i}$, $\mathbf{b_i}$	shunt conductance and susceptance at bus i
$\mathbf{z}_{ik}^0$	initial impedance of line ik, $\mathbf{z}_{ik}^0 = \mathbf{r}_{ik}^0 + \boldsymbol{j}\mathbf{x}_{ik}^0$
$\mathbf{r}_{ik}^0$, $\mathbf{x}_{ik}^0$	initial resistance and reactance of line ik
$\mathbf{I}_{ik}^{max,0}$	initial maximal allowed current flow of line ik
$\eta_{c,i}$,$\eta_{d,i}$	charging and discharging efficiency of storage at bus i
$\boldsymbol{c_{2,i}}$, $\boldsymbol{c_{1,i}}$, $\boldsymbol{c_{0,i}}$	cost coefficients for generator i
$\boldsymbol{c_{NEP,ij}}$, $\boldsymbol{c_{ij}}$	cost coefficient for network expansion of line ij
$\overline{\mathbf{y}}$	upper bound of a variable y
$\underline{\mathbf{y}}$	lower bound of a variable y

1 Introduction

1.1 Motivation

In recent years, distributed, as well as renewable energy generation have become more and more important on a medium voltage level. Additionally, to mitigate the associated volatility of the renewable energy sources (RES), storage systems are playing an increasing role in network operation. Fig. 1.1 illustrates such a distribution system, which are usually run in open ring structures, i.e. radial networks, [1], [2].

Moreover, the increase in demand and distributed generation (DG) stresses the exisisting distribution networks to the limits. Thus, network operators have to evaluate necessary network expansion taking these changes into account, [1], [2].

According to the German Energy Act [3], network operators need to guarantee a safe and reliable electricity supply at all times which includes the required demand as well as the technical physical constraints in the system. The goal in network operation and planning is to meet these requirements cost optimally.

The problem can be formulated as follows: How to allocate the power injection into the system, the expansion of existing power lines, and how to use storage systems, which introduce a temporal coupling to the problem, to find an optimal solution.

The problem is cast into a multiperiod optimal power flow (OPF) formulation. The OPF problem minimizes an objective function, e.g. total cost of the sytem, subject to physical and operational constraints in the network. It is usually a nonconvex nonlinear problem and, hence, hard to solve in general, e.g. [4],[5].

In earlier studies, a linearized OPF is solved for high voltage transmission networks. Assumptions that are made to linearize the OPF are acceptable considering transmission networks, but fail when it comes to medium voltage distribution grids, e.g. voltages across the network are not constant and line resistances are not negligibly small compared to line reactances [6], [7].

This motivates the analysis of a nonlinear multiperiod OPF in which the relevant features of modern distribution networks, such as RES and storage systems, are combined with the network expansion planning problem.

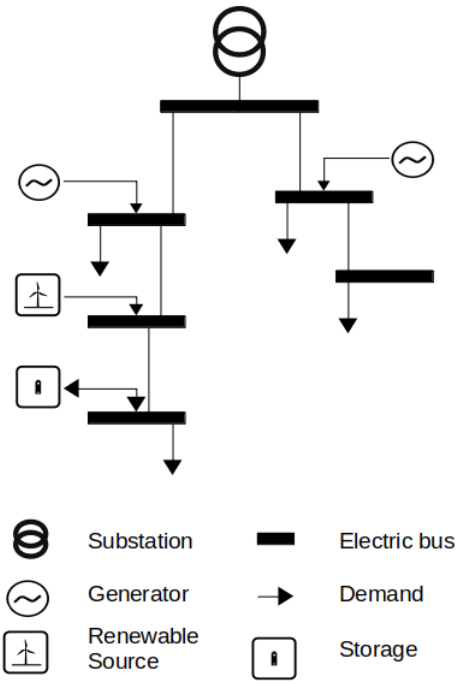

Figure 1.1: Schema of a distribution network

1.2 Problem formulation

In the following, the multiperiod OPF is introduced as the optimization programming which the work in this thesis is based on. At first, the necessary notations are described, followed by the objective function and physical and technical constraints.

1.2.1 Notations

The power network is represented as a connected directed graph $G = (N, E)$, where each node in N with $|N| = n + 1$ represents a bus and each edge in E with $|E| = m$ represents a distribution line. The power network is called *radial*

if G is a tree. The nodes are indexed by $i = 0, 1, \ldots, n$. Denote an edge by (i, k) if it connects node i with node k.

For each edge $(i, k) \in E$, let I_{ik} be the complex current and $S_{ik} = P_{ik} + \mathbf{j}Q_{ik}$ be the complex power flow between bus i and bus k, with P_{ik} and Q_{ik} denoting the active and reactive power flow, respectively. Furthermore, let $l_{ik} = |I_{ik}|^2$ be the squared magnitude current and I_{ik}^{max} be the current limit of the line between bus i and bus k. Additionally, let $z_{ik} = r_{ik} + \boldsymbol{j}x_{ik}$ be the complex impedance on the line between bus i and bus k with the resistance r and reactance x.

For each node $i \in N$, let $v_i = |V_i|^2$ be the squared magnitude voltage and $s_i = p_i + \boldsymbol{j}q_i$ be the complex power injection at bus i, with p_i and q_i denoting the active and reactive power injection, respectively. The active and reactive power injection consists of power generation and consumption $p_i \coloneqq p_i^g - p_i^c$ and $q_i \coloneqq q_i^g - q_i^c$. Additionaly, let $y_i = g_i - \boldsymbol{j}b_i$ be the complex shunt admittance from bus i to the ground with the shunt conductance g and shunt susceptance b.

The set of nodes with storage systems attached to them is denoted as S. For each node $i \in S$, let $u_{c,i}$, $u_{d,i}$, $\eta_{c,i}$, and $\eta_{d,i}$ be the charging and discharging rate, and the charging and discharging efficiency, respectively. Further, let e_i^t be the energy level of the storage at node i at time step t. For the power injection at nodes with storage systems the active power injection additionally consists of the discharging and charging rate, i.e. $p_i \coloneqq p_i^g - p_i^c + u_{d,i} - u_{c,i}$.

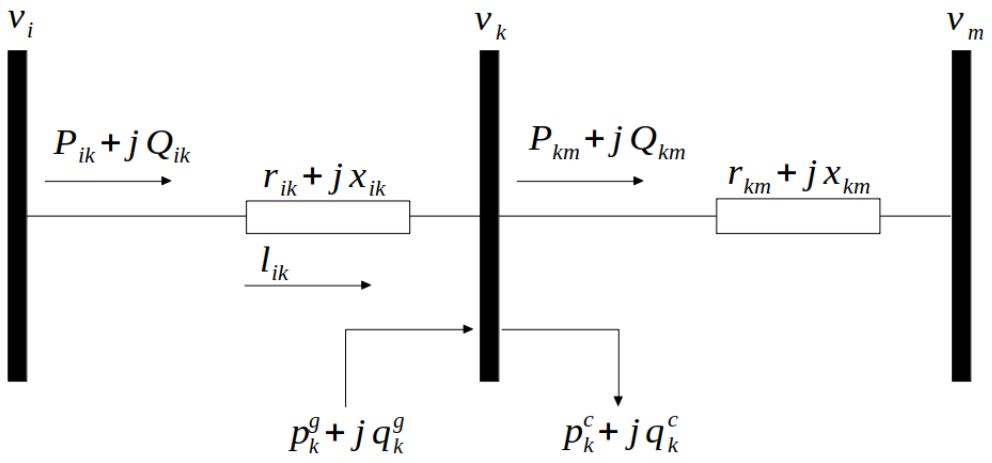

Figure 1.2: Power flow between three buses i, k, and m described in the line model adapted from [8]

1.2.2 Multiperiod OPF Problem Formulation

The goal is to minimize total network expansion and generation costs that arise with the integration of distributed generators and new loads, considering storage and possible curtailment that in conventional network planning are only rarely taken into account. In order to sufficiently incorporate these into grid planing a multiperiod OPF is introduced based on the followoing optimization programming:

$$\min_{\substack{p_g^t, q_g^t, v^t, \\ \ell^t, P^t, Q^t, I^{max}}} \quad \sum_{(i,k)\in E} C_{NEP}\left(I_{ik}^{max}\right) + \sum_{t\in\mathcal{T}}\sum_{i\in N} C_g\left(p_{g,i}^t\right) \tag{1.1}$$

s.t. $(\forall t \in \mathcal{T})$

$$p_k = \sum_{m:k\to m} P_{km} - \sum_{i:i\to k}\left(P_{ik} - r_{ik}\ell_{ik}\right) + g_k v_k, \qquad \forall k \in N \tag{1.2}$$

$$q_k = \sum_{m:k\to m} Q_{km} - \sum_{i:i\to k}\left(Q_{ik} - x_{ik}\ell_{ik}\right) - b_k v_k, \qquad \forall k \in N \tag{1.3}$$

$$v_k = v_i - 2\left(r_{ik}P_{ik} + x_{ik}Q_{ik}\right) + \left(r_{ik}^2 + x_{ik}^2\right)\ell_{ik}, \qquad \forall (i,k) \in E \tag{1.4}$$

$$v_i \ell_{ik} = P_{ik}^2 + Q_{ik}^2, \qquad \forall (i,k) \in E \tag{1.5}$$

$$\ell_{ik} \le |I_{ik}^{max}|^2 \qquad \forall (i,k) \in E \tag{1.6}$$

$$r_{ik} I_{ik}^{max} = \boldsymbol{r_{ik}^0 I_{ik}^{max,0}} \qquad \forall (i,k) \in E \tag{1.7}$$

$$x_{ik} I_{ik}^{max} = \boldsymbol{x_{ik}^0 I_{ik}^{max,0}} \qquad \forall (i,k) \in E \tag{1.8}$$

$$u_{c,i} u_{d,i} = 0 \qquad \forall i \in S \tag{1.9}$$

$$\boldsymbol{T_s}\left(\boldsymbol{\eta_{c,i}} u_{c,i}^t - \frac{u_{d,i}^t}{\boldsymbol{\eta_{d,i}}}\right) = e_i^{t+1} - e_i^t \qquad \forall i \in S \tag{1.10}$$

$$e_i^0 = e_i^{T+1} \qquad \forall i \in S \tag{1.11}$$

$$0 \le u_{c,i} \le \overline{\boldsymbol{u_{c,i}}}, \quad 0 \le u_{d,i} \le \overline{\boldsymbol{u_{d,i}}}, \quad 0 \le e_i^t \le \overline{\boldsymbol{e_i}} \qquad \forall i \in S \tag{1.12}$$

$$\underline{\boldsymbol{v_i}} \le v_i \le \overline{\boldsymbol{v_i}}, \quad \underline{\boldsymbol{p_i}} \le p_i \le \overline{\boldsymbol{p_i}}, \quad \underline{\boldsymbol{q_i}} \le q_i \le \overline{\boldsymbol{q_i}} \qquad \forall i \in N \tag{1.13}$$

The total system costs consists of the generation cost function $C_g\left(p_i^g\right) = \boldsymbol{c_{2,i}} p_{g,i}^2 + \boldsymbol{c_{1,i}} p_{g,i} + \boldsymbol{c_{0,i}}$ and the network expansion cost function $C_{NEP}\left(I_{ik}^{max}\right) = \boldsymbol{c_{NEP,ij}} I_{ik}^{max}$ over a given time horizon $\mathcal{T} = \{0, \ldots, T\}$, in which the time step of length T_s is denoted as t. The objective function is then given in (1.1).

The line model in Fig. 1.2 is used to set up the branch flow model (BFM) (constraints (1.2)-(1.5)) proposed in [9] and will be explained in more detail in section 3.1.

Constraint (1.2) and (1.3) represent the active and reactive power balance constraints at each node k, respectively. The first sum describes all the outgoing

lines from and the second sum all the incoming lines to node k. The term $r_{ik}\ell_{ik}$ ($x_{ik}\ell_{ik}$) accounts for the active (reactive) power losses over the line (i, k).

Constraint (1.4) contains Ohm's law and constraint (1.5) relates the power flow and current magnitude over a line (i, k). The latter is a quadratic equality constraint and introduces a nonconvexity into the problem.

Constraint (1.6) limits the squared magnitude current over a line. Constraints (1.7) and (1.8) describe the dependency of the resistance and reactance on the maximal current value of lines in parallel circuits, respectively, and are derived in section 3.2.

To reduce the general complexity of the problem, a continuous variable I_{ik}^{max} is considered to account for network expansion in the system, rather than a mixed integer approach proposed in other literature, see e.g. in [10]. The transition between those approaches is explained in section 3.2. Additionally, instead of allowing network expansion between any possible two buses, only existing lines can be reinforced.

The complementary constraint (1.9) prevents the storage of simultaneous charging and discharging and constraint (1.10) controls the time coupled state-of-charge. Both constraints are proposed by Marley et al. in [11]. (1.11) represents a periodic end-value of the state-of-charge for storage systems.

technical upper bounds on the storage variables, and technical voltage, active and reactive power injection limits for each bus i are described in (1.12) and (1.13), respectively.

As the maximal current rating is a decision variable, so are the resistance and reactance of the lines, which introduces the quadratic constraints (1.6) - (1.8). Additionally, (1.2)-(1.4) become quadratic, as well. Furthermore, the complementary constraint (1.9) is a nonconvex constraint.

Thus, the above multiperiod OPF, (1.1)-(1.10), is a nonconvex, nonlinear optimization problem and hence, in general, hard to solve.

1.3 Overview of thesis

This thesis is organized as follows. Chapter 2 includes a short literature overview regarding the optimal power flow problem. This overview includes representations of power flow equations and their relaxations, the network expansion problem, and storage modelling in multiperiod optimal power flow problems.

Chapter 3 gives some theoretical background on the problem examined in

this thesis, including a description of the branch flow model, the derivation of the network expansion representation proposed in this thesis, and mathematical background of second-order cone programming.

The test networks and data on which all numerical studies are performed, as well as the used solver are described in Chapter 4. In Chapter 5 a mixed integer representation of network expansion is compared to the approach presented in this thesis.

Chapter 6 explores relaxations of the optimal power flow problem analysed in this thesis. Sufficient conditions are provided to guarantee exactness of a second-order cone relaxation of the OPF including network expansion. Additionally, a McCormick relaxation is used on the current limit constraint.

The relaxations introduced in Chapter 6 are applied on the original multi-period optimal power flow including network expansion and storage systems and a computational study is performed in Chapter 7 including a sensitivity analysis considering network expansion costs.

A summary of the thesis as well as directions of possbile further research are given in Chapter 8.

2 Literature Overview

The goal of the OPF problem is to optimize a given planning or operational objective by controlling the power flow within the electrical system and the physical and technical constraints. Possible objective include for instance minimizing generation costs, minimizing losses in the system, or minimizing network expansion costs [4]. The first formulation of the problem was proposed by Carpentier [12] in 1962. The OPF determines the dispatch of power injection, the node voltages, current, and power flow throughout the system with respect to the power flow equations.

In general, the OPF problem is a nonlinear, nonconvex, large-scale optimization problem which may contain both continuous and discrete control variables. It is solved for many applications, such as long-term planning, day-ahead scheduling, real-time dispatch, et cetera. [5, 13, 4, 14]

In the following, an overview of state-of-the-art in grid operation and planning research is presented to motivate the decisions that are made for the multiperiod OPF formulation used in this thesis and introduced in section 1.2.

2.1 Power flow equations

The key constraints of the OPF problem are the power flow equations which model the fundamental electrical laws, such as the Ohm's Law and the Kirchoff's Current Law. They are, however, nonlinear and nonconvex [5], [13].

There are two traditional representation of the power flow equation. The bus injection model (**BIM**) focuses on the power injection and the voltage angle differences at the buses. The complex variables, e.g. voltage variables, can be expressed in either rectangular ($V = V_d + \boldsymbol{i}V_q$) or polar form ($V = |V| \exp^{\boldsymbol{i}\theta} \equiv |V|\angle\theta$), see surveys [5, 13, 14] for detailed description.

The branch flow model (**BFM**) concentrates on the quantities on the lines between the buses in the networks. It was first proposed by Baran and Wu in 1989 [15] for radial distribution networks and extended to transmission networks

by Coffrin in 2018 [16].

As it is designed for distribution networks in particular, and as mentioned later on, has beneficial numerical characteristics compared to BIM, power flow equations are represented by the BFM throughout this thesis, see 1.2, and are derived in 3.1.

2.2 Classical optimization

A variety of classical continuous deterministic optimization methods have been applied to solve the OPF problem. The survey [14] gives a detailed overview of the used optimization techniques. They include, e.g. gradient methods, Newton's method, and the interior point method. As gradient methods do not evaluate 2^{nd} order derivatives, they guarantee to find stationary points only, which can be local or global optima for well-behaved (convex) problems. The 2^{nd} order Newton's method and the interior point method also guarantee local optimality at most, due to the complexity of the general problem.

To find a global optimum of a multiperiod OPF, [17] propose a Branch-and-Bound algorithm using a convex relaxation as the lower and the local interior point method as the upper bound on the BIM.

2.3 Convex Relaxation

In recent years, **convex relaxations** of the power flow equation have been become more and more popular to solve the OPF to global optimality. Those relaxations enclose the nonconvex feasible space, spanned by the power flow equations, and then use the fundamental property of convex optimization problems to solve the problem, i.e. any locally optimal point is also globally optimal [18].

This results in three advantages. Firstly, if the relaxed problem is not feasible, the original problem is neither. Secondly, if an optimal solution is found, the relaxation gives a lower (upper) bound of the original minimization (maximization) problem. And finally, if the optimal solution found in the relaxation is feasible in the original problem, the solution is guaranteed to be a globally optimal solution of the original problem.

Comprehensive surveys of applied convex relaxation to various OPF formulations are given in [5] and [4]. There is always a trade off between having a

relaxation which is easy to find but gives a insufficient lower bound, and having a relaxation which encloses the feasible space of the original problem with the smallest convex set, the *convex hull* [1] which may be hard to find. Some of the key findings collected in the survey [5] and others regarding the relaxations of the power flow equations are presented in the following.

In the BIM the power flow equations are quadratic polynomials in terms of the complex voltage variables. This nonconvexity is often casted into one constraint by introducing a new variable $W = V\,(V^*)^T$, where $V = [V_1, \ldots, V_n]^T$ represents the collection of voltages, and V^* denotes the complex conjugate of V, so W is a positive semi-definite matrix and has rank 1. The literature focuses on finding relaxation for this particular constraint, including semidefinite programming (**SDP**) or second-order cone programming (**SOCP**). See [19] for an overview.

SDP relaxation

To from an SDP relaxation of the power flow equation, the nonconvex constraint $W \succeq 0$ and $\text{rank}(W) = 1$ is replaced by dropping the rank constraint resulting in the less stringent constraint $W \succeq 0$.

If the optimal solution $\widehat{W}$ of this relaxation satisfies the rank condition, the solution is exact and the decision variables can be recovered. Thus, the exactness of the relaxation is checked a posteriori. For a variety of the IEEE test cases [20] the SDP relaxation of the OPF tends to be exact, but fails for others [5]. The exactness is influenced by the choice of the objective function, where minimizing functions of active power generation tend to result in exactness more often [5].

Two sufficient conditions for exactness of the SDP relaxation can be found in the literature. Firstly, SDP relaxation becomes exact in weakly cyclic meshed networks, with a "load-oversatisfaction" assumption, i.e. no lower limits on the power injection, which means that power consumption can arbitrarily increase. Secondly, assumption of lossless networks that are (1) cycles with at most one *chord* [2] and (2) only have voltage magnitude constraints. [5]

[1] The convex hull of a set C, denoted $\mathbf{conv}\,C$, is the set of all convex combinations of points in C, $\mathbf{conv}\,C = \{\theta_1 x_1 + \cdots + \theta_k x_k | x_i \in C, \theta_i \geq 0, i = 1, \ldots, k, \theta_1 + \cdots + \theta_k = 1\}$ [18]

[2] In graph theory, a chord can be seen as a shortcut, that reduces a path between a vertex v to a vertex w to a shorter chordless path between these two vertices, see [21]

SOCP relaxation

The SOCP relaxation of the power flow equation in the BIM, proposed in [22], again introduces a new variable W_{ij} for the squared voltage magnitudes, where $W_{ij} = V_i V_j^*$ for all $i, j \in N \times N$, but convexifies each constraint seperately to a quadratic inequality, i.e. $|W_{ij}|^2 \leq W_{ii} W_{jj}$ for all $(i, j) \in E$.

Another SOCP relaxation is proposed for the BFM, which concentrates on the quadratic equality constraint of the power flow over the lines, see equation (1.5). By relaxing the equality to an inequality constraints, one obtains a rotated SOCP (see section 3.3), i.e.

$$v_i \ell_{ik} = P_{ik}^2 + Q_{ik}^2 \quad \Rightarrow \quad v_i \ell_{ik} \geq P_{ik}^2 + Q_{ik}^2$$

In [23] it is proven that there is a one-to-one mapping between the SOCP of the BFM and the SOCP of the BIM, so they are equivalent, but SOCP of the BFM has shown beneficial numerical characteristics compared to the SOCP of the BIM, [23],[11].

According to [24], the SDP relaxation is the strongest among the mentioned relaxations and exact for many cases, but for large-scale problems, the SOCP relaxation outperforms the SDP in terms of computational efficiency. Therefore, they propose a new conic relaxation, combining SDP and the reformulation-linearization technique (RLT) on the voltage products $|V_{ij}| = |v_i||v_j|$, by defining the convex hull of this product. Experiments show that this approach results in a stronger relaxation than the SOCP, and smaller solution time compared to the SDP relaxation.

[25] provides a number of sufficient conditions under which the SOCP relaxation, for both BIM and BFM, may be exact. In radial networks the SOCP relaxation becomes exact, if (1) there are no lower bounds on the power injection, also called "load oversatisfaction", (2) there are no upper bounds on the voltages, or (3) there is either no reverse power flow[3] or reverse power flow consisting only reactive or active power.

As those conditions may be reasonable when considering an operational OPF problem, they become meaningless if one considers a planning OPF problem such as the network expansion problem. Network expansion is done when 1) the lines between buses are overloaded and/or 2) the voltage bounds are violated, [6].

[3] In radial networks no reverse power flow means there is no power flowing towards the substation. [26]

If one allows load oversatisfaction, every surplus in the distributed - in particular renewable - energy sources would be drained at some bus just to avoid network expansion and not used in different parts of the network or in the superior network. If there are no upper bound on the voltages, the second reason to expand the network, the voltage violations, would be futile. Finally, as distributed volatile energy sources and storage systems are considered, a unidirectional power flow is not likely.

[27] provide sufficient conditions under which SOCP relaxation is guaranteed to be exact in radial networks for an operational OPF problem, these conditions are introduced and verified for the network expansion problem in Chapter 6.

2.4 Network expansion

As mentioned, there are mainly two reasons for network expansion: (1) Violation of the thermal limit of existing lines, i.e. overloading, or (2) violation of voltage bounds at nodes.

The planning process can be distinguished in single-stage or multi-stage process. In the single-stage scenario, the goal is to plan where to install new lines for a single case, whereas the multi-stage scenario also considers, when to expand the lines [10].

Network expansion is usually approached by solving a mixed integer problem (**MIP**), described for example in [10] and [4]. It can be distinguished between a multiple parallel line model (**MPLP**), see Section 3.2, and a binary MIP formulation.

The MPLP is presented for instance in [10]. An integer variable $n_{ij} \in \mathbb{Z}$ for all $(i, j) \in E$, representing the number of parallel lines between bus i and bus j, and a binary variable $\alpha^{(k)}$, equal to one if the kth line is build, are introduced.

A multistage binary MIP is proposed in [28], by defining possible line installation options y between bus i and j. The value of y then represents the number of lines installed between the to buses. A binary variable $w_{ij,y,t}$ indicates which option is used at each stage t. Additionally, it is made sure that once an option y at a stage $t-1$ is chosen, the number of lines between bus i and j is greater than or equal to that option at stage t, as lines cannot be removed later in the process.

Another approach to solve the network expansion problem is to define a number of worst cases, namely *load case* and *feed-in case*, and then perform an

iterative unconstraint power flow simulation with fixed power injection and consumption throughout the network. Following each simulation, lines are either reinforced or new lines are installed to tackle violation of thermal limits and voltage bounds, respectively [6].

2.5 Energy storage systems

When considering energy storage systems, a temporal coupling is introduced to the problem since a storage can only be discharged if charged in an earlier stage and vice versa. An overview of literature on multiperiod OPF models including storage systems is given for example in [29]. In [29], a number of key features are mentioned how storage systems are handled in multiperiod OPF.

An important constraint is the end-value constraint representing the capacity stored in the storage at the end of the considered time horizon. In literature it is for example distinguished between fixed values for the state-of-charge E at the time boundaries, periodic boundaries, i.e. $E_0 = E_T$ or a minimal state of charge at the end, $E_T \geq E_T^{min}$. Another feature is the considered time-horizon. Most of the reviewed literature considers a 24-h planning horizon.

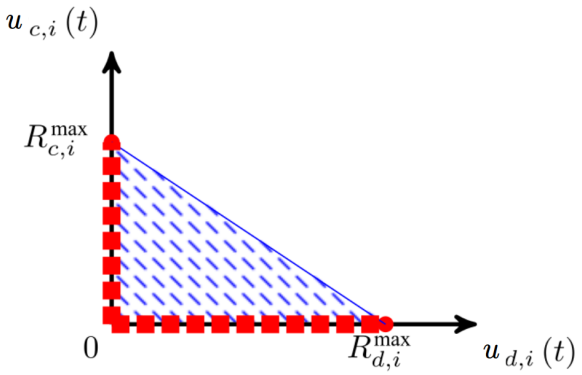

Figure 2.1: Feasible region of complementary constraint (1.9) (red dashed lines), and its convex hull (2.1) (blue), [11]

The storage dynamics are represented either through a single variable for charging (negative, power extracted from the network) and discharging (positive, power introduced into the network), e.g. [30], or through two variables denoting charging, u_c, and discharging, u_d, rate, e.g. [11]. The latter approach introduces a complementary constraint to avoid similtaneuous charging and discharging, i.e. $u_c u_d = 0$. In [11] the nonconvex complementary constraint of the

charging/discharging rate is then relaxed by introducing the convex hull of the constraint, which is illustrated in Fig. 2.1:

$$u_{c,i}^{t} u_{d,i}^{t} = 0 \quad \Rightarrow \quad u_{c,i}^{t} \leq - \left(\frac{R_{c,i}^{max}}{R_{d,i}^{max}} \right) u_{d,i}^{t} + R_{c,i}^{max} \tag{2.1}$$

To capture both the charging and discharging behaviour of the problem, especially since they will become more detailed and sophisticated, e.g. in [31], the "two variable" representation including its relaxed complementary constraint is used throughout this thesis.

3 Theoretical Background

This chapter introduces the theoretical background necessary to understand the OPF formulation which is introduced in section 1.2. First, the power flow equation in form of the branch flow model are explained in more detail.

Afterwards, the transformation of a mixed integer programming to a continuous representation of the network expansion problem is described.

The theoretical background is completed by presenting the normal form of the second-order cone programming as fundamental principles needed for the analytical study in chapter 6.

3.1 Branch Flow Model

As mentioned, the BFM was first proposed by Baran and Wu in [15] for radial networks. Let $G = (N, E)$ be a connected directed tree, where each node in N with $|N| = n + 1$ represents a bus and each edge in E with $|E| = m$ represents a distribution line.

In general, the power flow equations contain complex variables such as the complex voltage V, the complex current I, the complex power injection $s = p + \boldsymbol{j}q$, where p and q denote the active and reactive power injection, respectively, and the complex apparent power flow $S = P + \boldsymbol{j}Q$, where P and Q denote the active and reactive power flow, respectively. Additionaly, each edge (i, j) has a complex line impedance $z_{ij} = r_{ij} + \boldsymbol{j}x_{ij}$, and nodes may have a complex shunt admittance $y_i = g_i + \boldsymbol{j}b_i$. Moreover, let A^* denote the complex conjugate of complex variable A.

For each node i and each edge (i, j), the variables (S, I, V, s) have to satisfy Ohm's law

$$V_i - V_j = z_{ij} I_{ij}, \quad \forall (i, j) \in E\,, \tag{3.1}$$

the definition of the branch power flow

$$S_{ij} = V_i I_{ij}^*, \quad \forall (i, j) \in E\,, \tag{3.2}$$

and the power balance at each bus $j \in N$

$$\sum_{m:j\to m} S_{jm} - \sum_{i:i\to j} \left(S_{ij} - z_{ij} \left|I_{ij}\right|^2\right) + y_j^* \left|V_j\right|^2 = s_j \,. \tag{3.3}$$

Substituting (3.2) into (3.1) yields:

$$V_j = V_i - z_{ij} \frac{S_{ij}^*}{V_i^*}, \quad \forall (i,j) \in E \tag{3.4}$$

Taking the magnitude squared of (3.2) and (3.4), writing the equation in terms of real variable, one obtains the following branch flow model:

$$\begin{aligned}
p_j &= \sum_{m:j\to m} P_{jm} - \sum_{i:i\to j} \left(P_{ij} - r_{ij} \left|I_{ij}\right|^2\right) + g_j \left|V_j\right|^2, && \forall j \in N \\
q_j &= \sum_{m:j\to m} Q_{jm} - \sum_{i:i\to j} \left(Q_{ij} - x_{ij} \left|I_{ij}\right|^2\right) - b_i \left|V_j\right|^2, && \forall j \in N \\
\left|V_j\right|^2 &= \left|V_i\right|^2 - 2\left(r_{ij}P_{ij} + x_{ij}Q_{ij}\right) + \left(r_{ij}^2 + x_{ij}^2\right)\left|I_{ij}\right|^2, && \forall\,(i,j) \in E \\
\left|I_{ij}\right|^2 &= \frac{P_{ij}^2 + Q_{ij}^2}{\left|V_i\right|^2}, && \forall\,(i,j) \in E
\end{aligned}$$

The notation of $\ell_{ik} = \left|I_{ij}\right|^2$ and $v_i = \left|V_i\right|^2$ results in the BFM described in (1.2) - (1.5) in section 1.2 and is derived from [9]. In the literature, it is often called *relaxed branch flow model*, as information of the voltage and current angles, $\angle V_i$ and $\angle I_{ij}$, respectively, are lost, and the set of variables (P, Q, v, ℓ) is a subset of the complex variables (S, V, I), see e.g [9], [23], [25]. However, in [9] it is proven that for radial networks, i.e. G is a tree, one can easily recover the angles from the solution of the *relaxed BFM*. Therefore, the term BFM is used for the power flow equation in (1.2) - (1.5) throughout this thesis.

3.2 Network Expansion

In this section, the multiple parallel line model is introduced, followed by a short description of the behaviour of resistors and inductors in parallel circuits to explain the transition from a MINLP to an NLP formulation.

3.2.1 Multiple Parallel Line Model

In the Multiple Parallel Line Model (MPLM), n similar parallel lines may be installed between any two buses i and k, as illustrated in Fig. 3.1. Each of those

lines has the same impendance $z = r + \boldsymbol{j}x$, apparent power flow $S = P + \boldsymbol{j}Q$, and current flow ℓ.

In this model, line impedances are technical parameters and fixed for each line. The power flow and current flow is bounded by the thermal limits of a particular line m, i.e. $\ell_{ik} \leq \overline{\boldsymbol{\ell}}_{\boldsymbol{ik}}$ and $|S_{ik}| \leq \overline{\boldsymbol{S}}_{\boldsymbol{ik}}$ for all lines (i,k) in E.

Again, each node i and each line (i,k) in E have to satisfy the power flow equation represented in the previous section 3.1, resulting in the following constraints, written in terms of real variables:

$$p_k = \sum_{m:k\to m} n_{km}P_{km} - \sum_{i:i\to k} n_{ik}\left(P_{ik} - r_{ik}\ell_{ik}\right) + g_k v_k, \qquad \forall k \in N \tag{3.5}$$

$$q_k = \sum_{m:k\to m} n_{km}Q_{km} - \sum_{i:i\to k} n_{ik}\left(Q_{ik} - x_{ik}\ell_{ik}\right) - b_k v_k, \qquad \forall k \in N \tag{3.6}$$

$$v_k = v_i - n_{ik}\left(2\left(r_{ik}P_{ik} + x_{ik}Q_{ik}\right) + \left(r_{ik}^2 + x_{ik}^2\right)\ell_{ik}\right), \qquad \forall\,(i,k) \in E \tag{3.7}$$

$$v_i\ell_{ik} = P_{ik}^2 + Q_{ik}^2, \qquad \forall\,(i,k) \in E \tag{3.8}$$

$$0 \leq \ell_{ik} \leq \overline{\boldsymbol{\ell}}_{\boldsymbol{ik}}, \quad \underline{\boldsymbol{p}}_{\boldsymbol{ik}} \leq p_{ik} \leq \overline{\boldsymbol{p}}_{\boldsymbol{ik}}, \quad \underline{\boldsymbol{q}}_{\boldsymbol{ik}} \leq q_{ik} \leq \overline{\boldsymbol{q}}_{\boldsymbol{ik}} \qquad \forall (i,j) \in E \tag{3.9}$$

$$1 \leq n_{ik} \leq \boldsymbol{n}_{\boldsymbol{max}}, \quad n_{ik} \in \mathbb{Z} \qquad \forall\,(i,k) \in E \tag{3.10}$$

As only whole number of lines can be installed, the constraints (3.5)-(3.7) containing the integer variable n and constraints become MINLP constraints. These constraints are denoted as Multiple Parallel Line Programming (MPLP). As MINLPs are, in general, harder to solve than NLP, this motivates the reformulation of the network expansion problem into a continuous NLP.

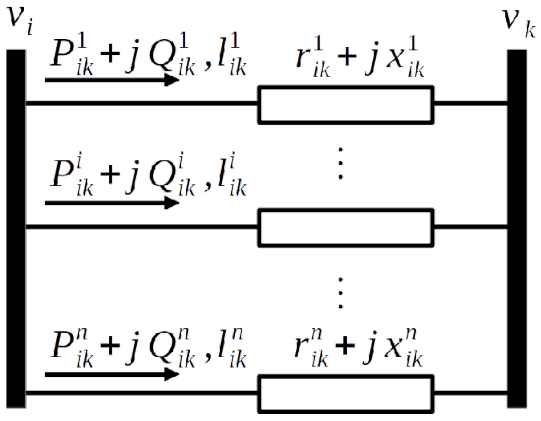

Figure 3.1: n lines installed between bus i and bus j

3.2.2 Continuous Network Expansion Problem

To transform the MPLP into an NLP, this section gives a short overview of the characteristics of two electrical components, resistance and inductor units, in parallel circuits, a detailed description of parallel circuits can be found in [32]. These characteristics are used to formulate an NLP for the network expansion problem. Fig. 3.2 illustrates parallel circuits of resistances R and inductors L.

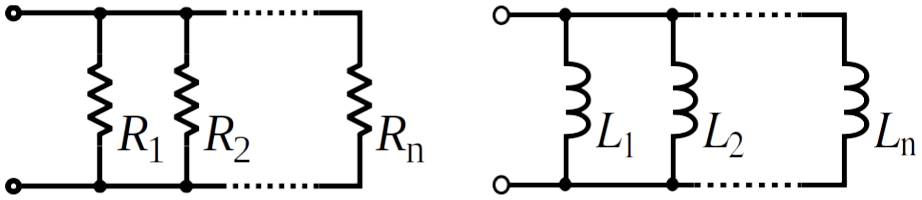

Figure 3.2: Resistances R_i (left) and inductors L_i (right) in parallel circuits

The total resistance R of such a circuit is obtained by summing the reciprocal values of all resistance units R_i in the parallel circuits.

$$\frac{1}{R} = \sum_{i=1}^{n} \frac{1}{R_i}$$

Considering N equal resistance units R_0 in the circuit the expression simplifies to

$$\frac{1}{R} = N\frac{1}{R_0} \quad \Leftrightarrow \quad R = \frac{1}{N}R_0 \tag{3.11}$$

The total inductance L is calculated for N equal non-coupled, i.e. the magnetic fields of the units do not interact with each other, inductor units L_0 analagously, resulting in

$$L = \frac{1}{N}L_0 \tag{3.12}$$

The reactance of a circuit x is propotional to its inductance and the nominal frequency of the current in the electrical power grid, i.e. 50 Hz in Germany, so (3.12) can be written as

$$x = \frac{1}{N}x_0 \tag{3.13}$$

Denote the maximal allowed current over a circuit as $I^{max,0}$ and consider N equal parallel circuits, than the total maximal allowed current, denoted as I^{max}, can be written as

$$I^{max} = NI^{max,0} \quad \Leftrightarrow \quad N = \frac{I^{max}}{I^{max,0}} \tag{3.14}$$

Plugging (3.14) into (3.11) and (3.13) with resistance in alternating currents $r = R$ yields the constraint given in (1.7) and (1.8)

$$rI^{max} = r^0 I^{max,0} \tag{1.7}$$

$$xI^{max} = x^0 I^{max,0} \tag{1.8}$$

By including the variable n from the MPLP in section 3.2.1 into the − as of now − variables r and x and letting the ratio of I^{max} and $I^{max,0}$ be continuous, the MPLP turns into an NLP, in which for each node i and for each line i, j in G the power flow equation (1.2) - (1.5) have to be satisfy with the set of variables $(P, Q, v, \ell, I^{max}, r, x)$. This NLP is the OPF formulation which is introduced in section 1.2 without storage systems for a single time step.

3.3 Second-order cone programming

A class of optimization problems is called second-order cone programming (SOCP). This section gives a basic understanding of this class which will be needed in Chapter 6. The SOCP can be represented as:

$$\begin{aligned} \min_{x} \quad & f^T x \\ \text{subject to} \quad & \|A_i x + b_i\|_2 \leq c_i^T x + d_i \quad i = 1, \ldots, m \\ & Fx \leq g, \end{aligned} \tag{3.15}$$

where $x \in \mathbf{R}^n$ is the optimization variable, $A_i \in \mathbf{R}^{n_i \times n}$, $F \in \mathbf{R}^{p \times n}$, and $\|\cdot\|_2$ denotes the 2-norm of a vector. The constraint of the form

$$\|Ax + b\|_2 \leq c^T x + d \tag{3.16}$$

where $A \in \mathbf{R}^{k \times n}$ is called a second-order cone constraint, since the affine function $\big(Ax + b, c^T x + d\big)$ lies in the set of the norm cone $C = \{(x, t) \,|\, \|x\| \leq t\} \subseteq \mathbf{R}^{k+1}$. The SOCP is **convex**, hence, each locally optimal solution is also a globally optimal solution, for a more detailed description see [18]. Figure 3.3 illustrates the boundary of a second-order cone in $\mathbf{R}^3$ where the interior of the cone describes the feasible space of the constraint.

In Chapter 6, nonconvex equality constraint of the branch flow (1.5) is relaxed to an inequality constraint. Any constraint of the form $\|u\|_2 \leq ab$, with any vector u, and $a \geq 0$, $b \geq 0$ can be represented as a rotated second-order cone

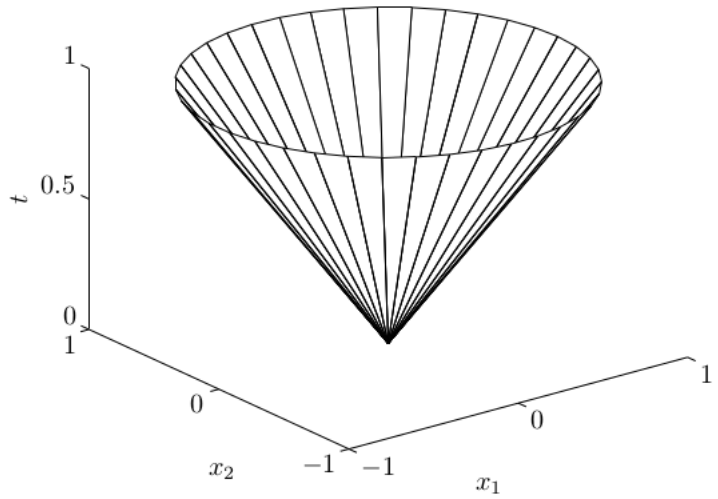

Figure 3.3: Boundary of second-order cone in $\mathbf{R}^3$, $\left\{(x_1, x_2, t) \,|\, (x_1^2 + x_2^2)^{1/2} \leq t\right\}$ where the interior of the cone describes the feasible space[18]

(SOC) constraint by the transformation to

$$\left\| \begin{bmatrix} 2u \\ a - b \end{bmatrix} \right\|_2 \leq a + b, \tag{3.17}$$

since

$$\begin{aligned} & \left\| \begin{bmatrix} 2u \\ a - b \end{bmatrix} \right\|_2^2 \leq (a + b)^2 \\ \Leftrightarrow \quad & 4\|u\|_2 + a^2 - 2ab + b^2 \leq a^2 + 2ab + b^2 \\ \Leftrightarrow \quad & 4\|u\|_2 \leq 4ab \\ \Leftrightarrow \quad & \|u\|_2 \leq ab. \end{aligned}$$

Hence, the relaxation of the nonconvex equality constraint of the branch flow (1.5) can be represented as an SOC constraint.

4 Test Networks and Solver

In the following, the data and solver which are used throughout my thesis are described. All numerical studies performed are based on two radial IEEE networks used in [33] and provided through the NESTA library, a collections of established power network test cases [34]. With these test networks various OPF problems are created.

4.1 Test cases

In this work, all problem formulations are applied on two radial networks containing 30 and 57 buses. In the following, data for these networks are provided.

4.1.1 30 Bus Case

The 30 bus network contains − beside the substation at bus 1 at which the slack is set − five distributed generators with a maximal active power capacity of 5.4 MW against a peak active load of 1.417 MW and peak reactive load of 0.63 MVAR.

Throughout this thesis, the active power output of generators at the buses 11 and 13 will be fixed to simulate non-dispatchable generation, e.g. volatile renewable energy sources which need to be allowed to inject all of their generated power.

The load and generation data is given in Table 4.2. The voltages of the buses are bounded with 0.94 p.u.[1] $\leq V_i \leq$ 1.06 p.u. for all buses in the network.

Table 4.1 summarizes the branch data of the 30 bus network. Transformers in the network are modelled through lines with resistance r equal zero. The network is illustrated in Fig. 4.1.

[1] p.u.: per unit

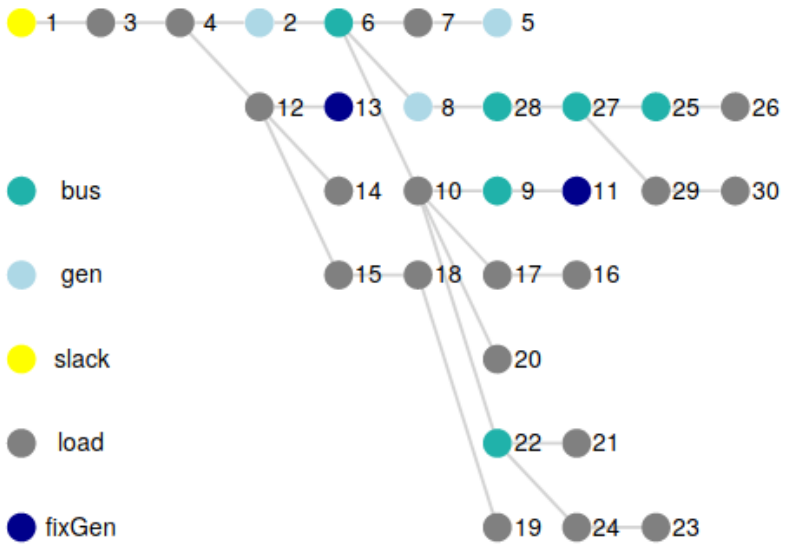

Figure 4.1: 30 bus network, the slack at substation bus 1, three dispatchable generators at bus $2, 5, 8$, two non-dispatchable generators at bus $11, 13$.

Table 4.1: Impedances and maximal allowed current of lines in 30 bus network

Branch Data

from bus	to bus	r^0 Ω	x^0 Ω	$I^{max,0}$ kA	from bus	to bus	r^0 Ω	x^0 Ω	$I^{max,0}$ kA
1	3	0.0452	0.1652	1.829	15	18	0.1073	0.2185	1.287
2	4	0.057	0.1737	1.712	18	19	0.0639	0.1292	2.170
3	4	0.0132	0.0379	7.776	10	20	0.0936	0.209	1.372
2	6	0.0581	0.1763	1.691	10	17	0.0324	0.0845	3.457
5	7	0.046	0.116	2.510	10	22	0.0727	0.1499	1.88
6	7	0.0267	0.082	3.627	21	22	0.0116	0.0236	11.872
6	8	0.012	0.042	7.148	22	24	0.115	0.179	1.468
6	10	0	0.556	0.563	23	24	0.132	0.27	1.042
9	11	0	0.208	1.510	25	26	0.2544	0.38	0.691
9	10	0	0.11	2.840	25	27	0.1093	0.2087	1.329
4	12	0	0.256	1.223	28	27	0	0.396	0.797
12	13	0	0.14	2.234	27	29	0.2198	0.4153	0.670
12	14	0.1231	0.2559	1.106	29	30	0.2399	0.4533	0.617
12	15	0.0662	0.1304	2.138	8	28	0.0636	0.2	1.489
16	17	0.0524	0.1923	1.574					

Table 4.2: Load and generation capacity of 30 bus network

Load Data						**Flexible generation**			
Bus No.	P_d MW	Q_d MVA	Bus No.	P_d MW	Q_d MVA	Bus No.	Q^g_{max} MVA	Q^g_{min} MVA	P^g_{max} MW
2	0.1085	0.0635	17	0.045	0.029	2	0.5	-0.3	1.4
3	0.012	0.006	18	0.016	0.0045	5	0.4	-0.3	1
4	0.038	0.008	19	0.0475	0.017	8	0.4	0	1
5	0.471	0.095	20	0.011	0.0035	**Fixed generation**			
7	0.114	0.0545	21	0.0875	0.056	Bus No.	Q^g_{max} MVA	Q^g_{min} MVA	P^g MW
8	0.15	0.15	23	0.016	0.008				
10	0.029	0.01	24	0.0435	0.0335	11	0.24	0	1
12	0.056	0.0375	26	0.0175	0.0115	13	0.24	0	1
14	0.031	0.008	29	0.012	0.0045	**Shunt capacitors**			
15	0.041	0.0125	30	0.053	0.0095	Bus	MVar	Bus	MVar
16	0.0175	0.009				10	0.19	24	0.043

$P_{peak} = 1.417$ MW $Q_{peak} = 0.63$ MW $V_{min} = 0.94$ $V_{max} = 1.06$

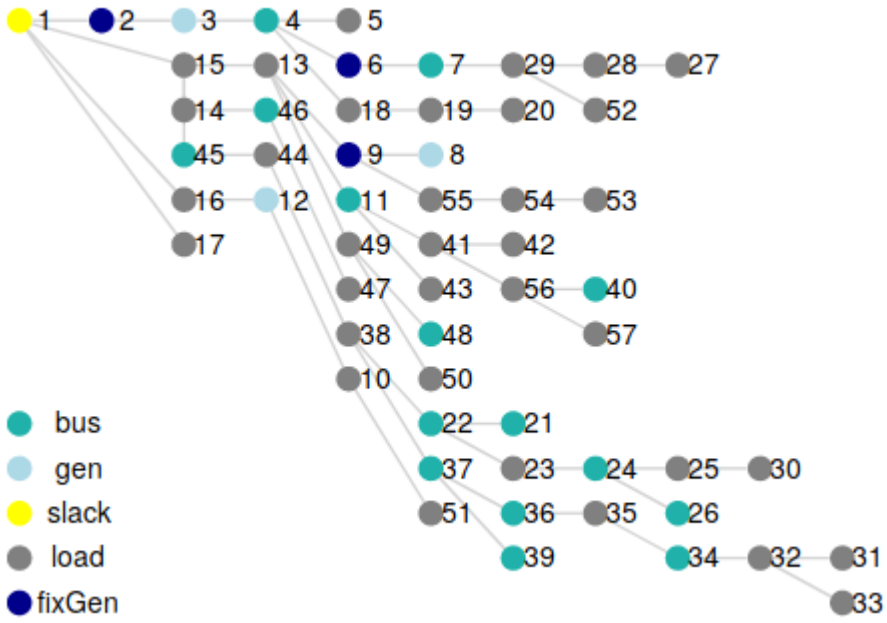

Figure 4.2: 57 bus network ,the slack at substation bus 1, three dispatchable generators at bus $4, 8, 12$, three non-dispatchable generators at bus $2, 6$,

4.1.2 57 Bus Case

The 57 bus network contains six generators. The generators at buses 2, 6, and 9 are fixed at their nominal active power generation of $p^g = 1$ MW. The total maximal capacity of the distributed generation in the network is 14 MW, whereas the peak load lies at 4.7 MW and 1.105 MVAR for the active and reactive part, respectively. The voltages are again bounded with $V_{min} = 0.94$ p.u. and $V_{max} = 1.06$ p.u. Table 4.3 summarizes the data of load and generation in the network and table 4.4 the line impedances and thermal limits. Again, transformers are modelled as lines with a resistance $r = 0$.

Table 4.3: Load and generation capacity of 57 bus network

Load Data						**Flexible generation**			
Bus No.	P_d MW	Q_d MVA	Bus No.	P_d MW	Q_d MVA	Bus No.	Q^g_{max} MVA	Q^g_{min} MVA	P^g_{max} MW
1	0.183	0.0557	29	0.057	0.0096	3	0.6	-0.2	1.4
2	0.01	0.2853	30	0.012	0.0067	8	2	-1.5	5.5
3	0.137	0.0682	31	0.019	0.0096	12	1.55	-1.6	4.1
5	0.043	0.0125	32	0.005	0.0029	**Fixed generation**			
6	0.25	0.0077	33	0.013	0.0067	bus No.	Q^g_{max} MVA	Q^g_{min} MVA	P^g MW
8	0.5	0.0711	35	0.02	0.0096	2	0.5	-0.27	1
9	0.403	0.0845	38	0.047	0.0221	6	0.25	-0.18	1
10	0.017	0.0077	41	0.021	0.0096	9	0.09	-0.13	1
12	1.257	0.0778	42	0.024	0.0154	**Shunt capacitors**			
13	0.06	0.0086	43	0.007	0.0029	Bus		MVar	
14	0.035	0.0173	44	0.04	0.0067				
15	0.073	0.0163	47	0.099	0.0384	18		0.1	
16	0.143	0.0096	49	0.06	0.0269	25		0.059	
17	0.14	0.0269	50	0.07	0.0346	53		0.063	
18	0.091	0.0317	51	0.06	0.0173	**Peak load**			
19	0.011	0.0019	52	0.016	0.0077	Active		Reactive	
20	0.008	0.0029	53	0.067	0.0317	MW		MVA	
23	0.021	0.0077	54	0.014	0.0058	4.7		1.105	
25	0.021	0.0106	55	0.023	0.0106	**Voltage bounds**			
27	0.031	0.0019	56	0.025	0.0077	$V_{min} = 0.94$			
28	0.015	0.0086	57	0.022	0.0077	$V_{max} = 1.06$			

Table 4.4: Impedances and maximal allowed current of lines in 50 bus network

Branch Data

from bus	to bus	r^0 Ω	x^0 Ω	$I^{max,0}$ kA	from bus	to bus	r^0 Ω	x^0 Ω	$I^{max,0}$ kA
1	2	0.0083	0.028	1.069	31	32	0.507	0.755	0.035
2	3	0.0298	0.085	0.347	32	33	0.0392	0.036	0.587
3	4	0.0112	0.0366	0.816	34	32	0	0.953	0.033
4	5	0.0625	0.132	0.214	34	35	0.052	0.078	0.333
4	6	0.043	0.148	0.203	35	36	0.043	0.0537	0.454
6	7	0.02	0.102	0.301	36	37	0.029	0.0366	0.669
8	9	0.0099	0.0505	0.606	37	38	0.0651	0.1009	0.261
9	13	0.0481	0.158	0.189	37	39	0.0239	0.0379	0.697
13	15	0.0269	0.0869	0.344	22	38	0.0192	0.0295	0.887
1	15	0.0178	0.091	0.337	11	41	0	0.749	0.043
1	16	0.0454	0.206	0.149	41	42	0.207	0.352	0.077
1	17	0.0238	0.108	0.283	38	44	0.0289	0.0585	0.479
4	18	0	0.555	0.056	15	45	0	0.1042	0.3
10	12	0.0277	0.1262	0.243	14	46	0	0.0735	0.426
11	13	0.0223	0.0732	0.409	46	47	0.023	0.068	0.435
12	16	0.018	0.0813	0.376	48	49	0.0834	0.129	0.203
14	15	0.0171	0.0547	0.545	49	50	0.0801	0.128	0.207
18	19	0.461	0.685	0.038	10	51	0	0.0712	0.438
19	20	0.283	0.434	0.061	13	49	0	0.191	0.164
21	22	0.0736	0.117	0.227	29	52	0.1442	0.187	0.133
22	23	0.0099	0.0152	1.72	53	54	0.1878	0.232	0.105
23	24	0.166	0.256	0.103	54	55	0.1732	0.2265	0.11
24	25	0	1.182	0.027	11	43	0	0.153	0.204
24	26	0	0.0473	0.661	44	45	0.0624	0.1242	0.226
27	28	0.0618	0.0954	0.276	40	56	0	1.195	0.027
28	29	0.0418	0.0587	0.434	56	41	0.553	0.549	0.04
7	29	0	0.0648	0.482	57	56	0.174	0.26	0.1
25	30	0.135	0.202	0.129	9	55	0	0.1205	0.26

4.1.3 Multiperiod Data

In both test networks, a number of generators has a fixed power value. To represent the increase in distributed generation, such as renewable energy sources, and their volatitily, a timeseries of a varying random scaling factor is introduced. This variation can be caused, for instance by the change in wind speed, when operating a wind farm. The power injection $p_{g,i}^t$ for all generators i in the set of the fixed generators are multiplied by this factor of timestep t. Fig. 4.3 shows the timeseries of the scaling factor used in this these for all instances.

Example: In the 30 bus case, generators at bus 11 and 13 have a nominal non-dispatchable power injection of 1 MW. For timestep $t = 4$ the scaling factor equals 1.6, resulting in an active power injection of $p_{g,i}^4 = 1.6$ MW for $i = 11$ and $i = 13$.

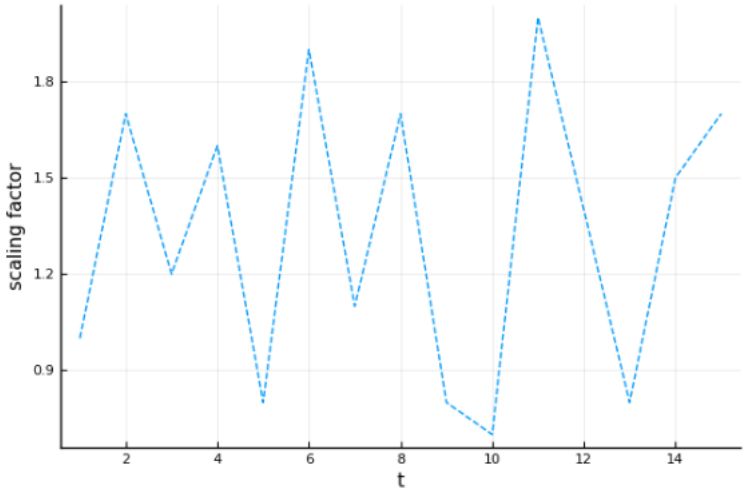

Figure 4.3: Scaling factor vs. time

4.2 Setup and solving

After building the test network architecture with the Julia package *PowerModels.jl* [35], the instances of the optimization problem are implemented using the package *JuMP.jl* [36].

As the created instances result in nonconvex MINLPs or NLPs, a suitable global solver is needed. For this, the non-commercial global solver for mixed integer nonlinear programm **SCIP v.6.0.1** [37] is used, which is based on a combined approach of *Branch-and-bound* and *LP relaxations* [38]. By emperical

observation, the implemented presolving was disadvantageous and is turned off. As local solver, the *Interior Point Method* [39] is primarily used. All simulations are performed on a HP ProBook with 2.60GHz Intel Core i5-4210M 1045 MHz and 8GB memory.

5 Network expansion – mixed integer vs. continuous formulation

In this chapter, three optimization problems considering a network expansion problem are compared for time horizons $\mathcal{T} \in \{1, 2, \ldots, 8\}$. The study is performed on the 30 bus and 57 bus network, described in section 4.1. In the following, the formulations are presented and the results of the computational experiments are shown and discussed.

5.1 Problem formulations

The problems are formulated as **MIP**, representing the MPLP introduced in Section 3.2.1, **cMIP**, a similar setup, but with a continuous interpretation of the network expansion variables, and **NLP**, described in section 3.2.2. The goal is to minimize the cost of expansion and cost of generation commitment. Only the **MIP** is a mixed integer formulation, the others are continuous.

$$\textbf{MIP:} \quad \min_{\substack{p_g^t, q_g^t, v^t, \\ \ell^t, P^t, Q^t, n_{ik}}} \sum_{(i,k)\in E} c_{ik} n_{ik} + \sum_{t\in\mathcal{T}} \sum_{i\in N} C_g\left(p_{g,i}^t\right) \tag{5.1}$$

s.t. $(\forall t \in \mathcal{T})$

$$(3.5) - (3.10)$$

$$\underline{\boldsymbol{v_i}} \leq v_i \leq \overline{\boldsymbol{v_i}}, \quad \underline{\boldsymbol{p_i}} \leq p_i \leq \overline{\boldsymbol{p_i}}, \quad \underline{\boldsymbol{q_i}} \leq q_i \leq \overline{\boldsymbol{q_i}} \quad \forall i \in N \tag{5.2}$$

$$\textbf{cMIP:} \quad \min (5.1)$$

s.t. $(\forall t \in \mathcal{T})$

$$(3.5) - (3.9), (5.2)$$

$$1 \leq n_{ik} \leq \boldsymbol{n_{max}}, \quad n_{ik} \in \mathbb{R} \qquad \forall (i,k) \in E$$

NLP: $\min (1.1)$

s.t. $(\forall t \in \mathcal{T})$

$(1.2) - (1.8), (5.2)$

5.2 Results

For all of the instances, a time limit of 1000 s and a primal-dual gap limit of 1 % is chosen. The primal-dual gap is defined by $gap\% = \frac{primal-dual}{primal} \times 100$.

5.2.1 30 Bus Case

Fig. 5.1 shows the solution time (left) of the instances and their primal-dual gap (right) for global optimality over the length of the considered time horizon for the 30 bus case.

Considering the MIP, a primal solution is found for a time horizon $\mathcal{T} = 1$ with a primal-dual gap of 24 % and a time limit of 1000 s. For longer time horizon no primal solution is found in the given time limit for the MIP.

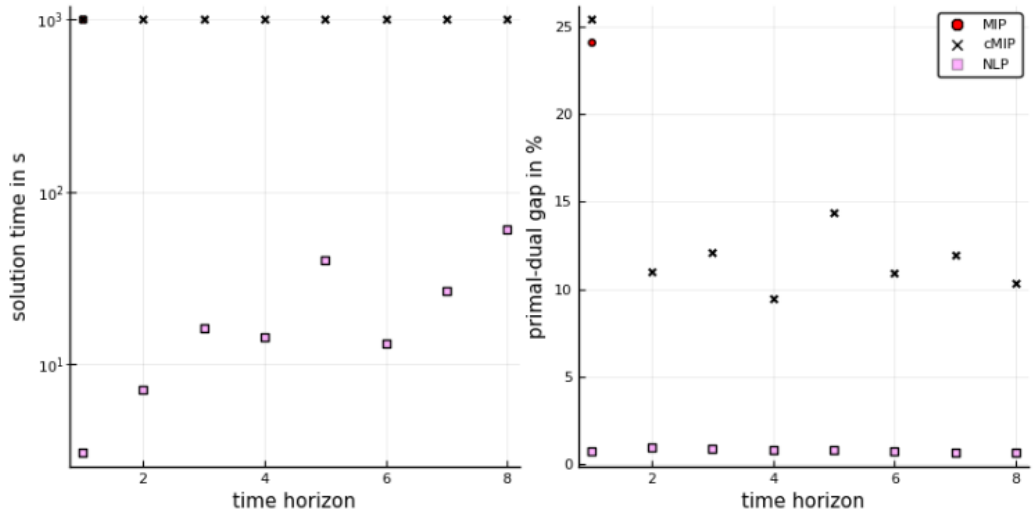

Figure 5.1: Computing time and primal-dual gap for solving **MIP** (circle), and the two continuous nonlinear problem **cMIP** (cross) and **NLP** (square) for different time horizons in a **30 bus** network to global optimality using **SCIP**. Time limit: 1000 s; Gap Limit: 1 %

For all optimized instances of the cMIP primal solutions are found. The lowest primal-dual gap is found for $\mathcal{T} = 4$ with < 10 %. For the rest of the instances

the primal-dual gap varies between 9 to 15 per cent.

For all instances in the NLP, the primal-dual gap of the solution can be closed up to at least 1 % in less than 100 s.

The final objective values of the three formulations are similar for each time horizon, i.e. all formulations find the same solution if a solution is found, shown in Table 5.1.

Table 5.1: Objective values of 30 bus case

$\mathcal{T}$	MIP	cMIP	NLP	gap = $\frac{\text{cMIP}-\text{NLP}}{\text{cMIP}}$
1	7945.9	7935.9	7934.8	1.39E-04
2	∞	19875.1	19816.6	2.94E-03
3	∞	28231.9	28172.6	2.10E-03
4	∞	39281.9	39225.9	1.43E-03
5	∞	45520.4	45460.6	1.31E-03
6	∞	58952.0	58859.3	1.57E-03
7	∞	66707.8	66614.4	1.40E-03
8	∞	78488.9	78396.4	1.18E-03

5.2.2 57 Bus Case

Fig. 5.2 shows the solution time (left) of the instances and their primal-dual gap (right) for global optimality over the length of the considered time horizons for the 57 bus case. Compared to the 30 bus case, SCIP manages to find solutions for multiple time horizons in the MIP formulation. Solutions are found for $\mathcal{T} = 1, 2, 3, 5$. After the time limit is reached, the primal-dual gap is close to 30 % for $\mathcal{T} = 1$ and around 15 % for the remaining ones.

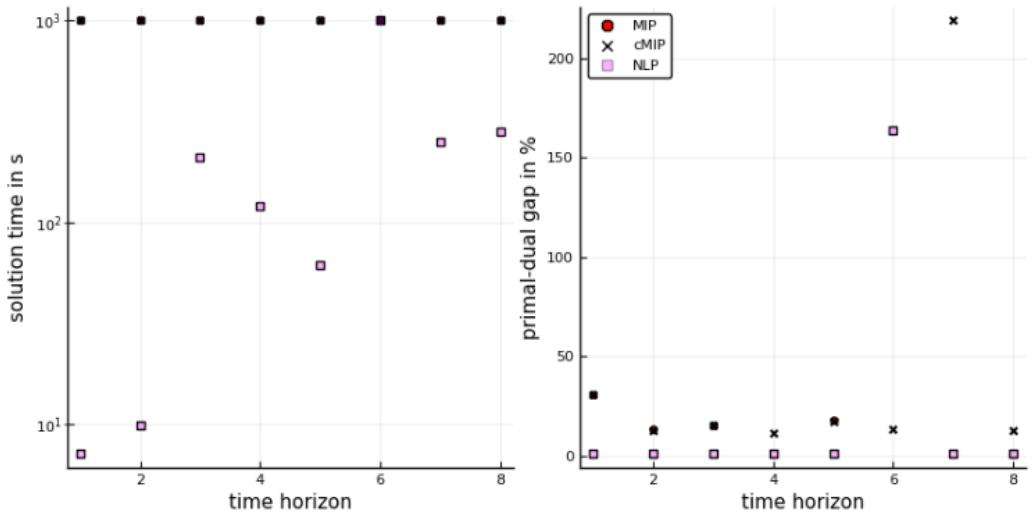

Figure 5.2: Computing time and primal-dual gap for solving **MIP** (circle), and the two continuous nonlinear problem **cMIP** (cross) and **NLP** (square) vs. the length of the considered timehorizon in a **57 bus** network to global optimality using **SCIP**. Time limit: 1000 s; Gap Limit: 1 %

In the cMIP a primal solution is found for every evaluated time horizon. The primal-dual gap at the time limit is similar to the ones of the MIP. For the time horizons 4, 6, and 8 the gap is closed upto 15 % as well. Only for the time horizon $\mathcal{T} = 7$, the primal-dual gap deviates strongly from the rest with a gap > 200 %.

For the NLP formulation the primal-dual gap is closed upto 1 % in less than 300 s, except in $\mathcal{T} = 6$ which results in a gap of > 150 % at 1000 s.

The strong deviation in the resulting primal-dual gap, i.e. MIP: $\mathcal{T} = 7$ and NLP: $\mathcal{T} = 5$, may result from choices of primal heuristics in SCIP. The primal solution of most of the instances is found by the local interior point method, but in these mentioned cases the large neighborhood search heuristic is used which

does not seem to be a good choice.

Again, for each single time horizon the three formulation find the same final objective value if a solution is found, shown in Table 5.2.

Table 5.2: Objective values of 57 bus case

$\mathcal{T}$	MIP	cMIP	NLP	gap = $\frac{\text{cMIP}-\text{NLP}}{\text{cMIP}}$
1	16883.7	16880.8	16874.3	3.82E-04
2	37200.3	37147.9	37132.1	4.25E-04
3	53504.3	53368.1	53345.2	4.29E-04
4	∞	72564.6	72535.3	4.05E-04
5	86690.5	86336.2	86301.3	4.04E-04
6	∞	108931.1	285616.2	-1.62E+00
7	∞	346026.5	124412.5	6.40E-01
8	∞	144632.4	144583.3	3.39E-04

5.3 Conclusion

Three formulation of an multiperiod Optimal Power Flow (OPF) including network expansion variables are compared on two test cases. As expected, the NLP outer performs the MIP formulation with respect to computation time, as mixed inter problems are, in general, harder to solve, but even compared to the cMIP, the NLP performs significantly better.

In both test networks, the NLP reduces the computation time by at least an order of ten, in order to find a solution and prove global optimality with up to 1 %. As all the formulation result in the same objective value and solution, if found, it is fair to say, that the NLP is good representation of the network expansion problem.

6 Convex Relaxations of OPF constraints

In this chapter, two relaxations of constraints of the OPF, (1.1) - (1.8), are described. First an SOCP relaxation of the branch flow constraint (1.5) and sufficient conditions, first proposed in [27], are provided which garuantee exactness of the relaxation in radial networks. Afterwards, the current limit constraint (1.6) is relaxed using the McCormick Envelopes.

6.1 Exact Convex Relaxation in Radial Networks

[27] propose a theorem for exactness of a SOCP relaxation under two conditions that can be checked 1) a priori and 2) a posteriori in [27]. The nonconvex equality constraint in (1.5) is relaxed to an inequality constraint, which can be reformulated as a rotated SOC constraint, see 3.3, i.e.:

$$v_i \ell_{ij} = P_{ij}^2 + Q_{ij}^2 \quad \Rightarrow \quad v_i \ell_{ij} \geq P_{ij}^2 + Q_{ij}^2 \tag{6.1}$$

SOCP is exact if every of its solutions obtains equality in 6.1 and, hence, satisfies (1.5). In the following, this theorem is introduced and a new proposition is formulated to extend the theorem by Gan et al. for the network expansion planning proposed in this thesis. Let

- The network $G = (N, E)$ be a tree.
- $N \coloneqq \{0, \ldots, n\}$ denote the set of nodes including the substation node 0, and $N^+ \coloneqq N \setminus \{0\}$.
- E denote the set of all lines in G.
- The substation voltage, denoted as v_0, be fixed and given.

- Line resistances and reactances be strictly positive, i.e. $r_{ij} > 0$ and $x_{ij} > 0$ for $(i,j) \in E$
- Voltage lower bounds be strictly positive, i.e. $\underline{v_i} > 0$ for all $i \in N$.

6.1.1 OPF in Radial Networks

Considering radial networks with orientation towards the substation bus 0, the optimization problem (1.1)-(1.8) for a single period without storage systems simplifies to

$$\min_{\substack{s_g,v,\\ \ell,S,I^{max}}} \quad \sum_{(i,j)\in E} c_{ij} I_{ij}^{max} + \sum_{i\in N} C_g\left(\mathrm{Re}(s_{g,i})\right) \tag{6.2}$$

subject to

$$s_j = S_{jm} - \sum_{i:i\to j} \left(S_{ij} - z_{ij}\ell_{ij}\right), \qquad \forall j \in N \tag{6.3}$$

$$s_0 = -\sum_{i:i\to j} \left(S_{i0} - z_{i0}\ell_{i0}\right), \qquad \forall j \in N \tag{6.4}$$

$$v_j = v_i - 2\mathrm{Re}\left(z_{ij}S_{ij}\right) + |z_{ij}|^2 \ell_{ij}, \qquad \forall\,(i,j) \in E \tag{6.5}$$

$$v_i \ell_{ij} \geq |S_{ij}|^2, \qquad \forall\,(i,j) \in E \tag{6.6}$$

$$\ell_{ij} \leq \left|I_{ij}^{max}\right|^2 \qquad \forall\,(i,j) \in E \tag{6.7}$$

$$r_{ij} I_{ij}^{max} = \boldsymbol{r_{ij}^0 I_{ij}^{max,0}} \qquad \forall\,(i,j) \in E \tag{6.8}$$

$$x_{ij} I_{ij}^{max} = \boldsymbol{x_{ij}^0 I_{ij}^{max,0}} \qquad \forall\,(i,j) \in E \tag{6.9}$$

6.1.2 Sufficient Condition

Assume lossless power flow, i.e. $z_{ij}\ell_{ij} = 0$ for all (i,j) in E, one obtains the solution of the *Linear DistFlow* [15], denoted as $(\hat{S}, \hat{v})$, with

$$\hat{S}_{ij}(s) = \sum_{h:i\in P_h} s_h, \qquad \forall (i,j) \in E; \tag{6.10}$$

$$\hat{v}_i(s) :== v_0 + 2\sum_{(j,k)\in P_i} \mathrm{Re}\left(z_{jk}S_{jk}\right), \qquad \forall i \in N \tag{6.11}$$

as illustrated in Fig. 6.1. Both $\hat{S}$ and $\hat{v}$ provide upper bounds on S and v, respectively [27] and are necessary for the proof of the following theorem.

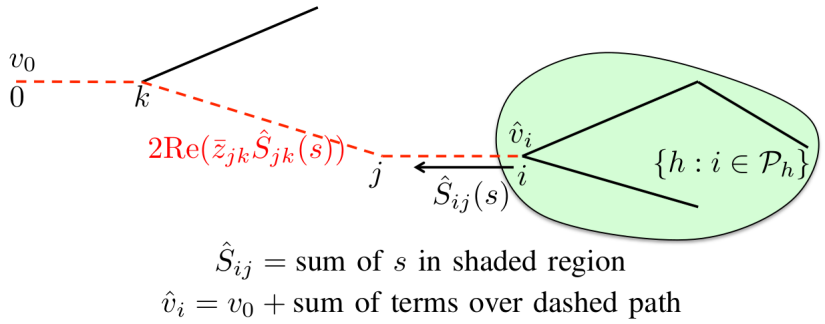

Figure 6.1: Illustration of $\hat{S}_{ij}$ and $\hat{v}_{ij}$, shaded region contains buses $\{h : i \in P_h\}$ downstream of bus i. Dashed lines describe the path P_i from bus i to bus 0 [27].

Physically, $\hat{S}_{ij}$ denotes the sum of power injections s_h in region P_h downstream of bus i, towards bus 0 that goes through line (i, j). Let $a^+ \coloneqq \max\{a, 0\}$ for $a \in \mathbb{R}$, $I \coloneqq \mathrm{diag}\,(1, 1)$ denote the 2×2 identity matrix, and define

$$u_i \coloneqq u_{ij} \coloneqq \begin{pmatrix} r_{ij} \\ x_{ij} \end{pmatrix}, \quad \underline{A}_i \coloneqq \underline{A}_{i,j} \coloneqq I - \frac{2}{\underline{v}_i} \begin{pmatrix} r_{ij} \\ x_{ij} \end{pmatrix} \begin{pmatrix} \hat{P}_{ij}^+(\overline{p}) & \hat{Q}_{ij}^+(\overline{q}) \end{pmatrix}$$

for (i, j) in E. Where $\hat{P}$ and $\hat{Q}$ denote the real and imaginary part of $\hat{S}$, and $\overline{p}$ and $\overline{q}$ denote the upper bounds of the real and imaginary part of the power injection s, respectively. At last, let $L \coloneqq \{l \in N | \nexists k \in N \text{ such that } k \to l\}$ denote the set of leaf buses in the network and P_l be the path from a leaf bus l to bus 0 with

$$P_l = \{l_{n_l} \to l_{n_l - 1} \to \cdots \to l_1 \to l_0\}$$

where $l_{n_l} = l$ and $l_0 = 0$ as illustrated in Fig. 6.2.

Theorem 1 (cf. [27]). *Assume that $C_g(s_0)$ is strictly increasing, and that there exists $\overline{p}_i$ and $\overline{q}_i$ such that $S_i \subseteq \{s \in \mathbb{C} | Re(s) \leq \overline{p}_i, Im(s) \leq \overline{q}_i\}$ for $i \in N^+$. Then SOCP is exact if the following conditions hold:*

C1 $\underline{A}_{l_s} \cdots \underline{A}_{l_{t-1}} u_{l_t} > 0$ for any $l \in L$ and any s, t such that $1 \leq s \leq t \leq n_l$,

C2 every SOCP solution $w = (s, S, v, \ell, s_0)$ satisfies $s \in S_{volt}$, where $S_{volt} \coloneqq \{s \in \mathbb{C}^n | \hat{v}(s) \leq v_i \text{ for } i \in N^+\}$

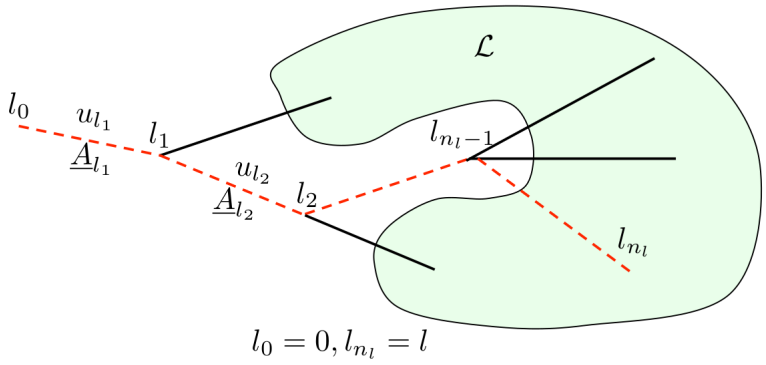

Figure 6.2: Shaded region contains set of leaf buses L, and the path P_l from leaf bus $l \in L$ to bus 0 as dashed lines [27].

Theorem 1 implies, that if the optimal power injections lie in the region S_{volt}, i.e. $C2$ holds, then SOCP is exact under $C1$. The theorem is proven in [27] by a "proof by contradiction", for the details the reader is referred to the original paper. Condition $C1$ is illustrated through a single feeder network with $n+1$ buses as in Fig. 6.3. In this network, the set of leaf buses L only contains the bus n, the unique path from n to bus 0 is $P_n = \{n \to n-1 \to \cdots \to 1 \to 0\}$, and $C1$ takes the form

$$\underline{A}_s \cdots \underline{A}_{t-1} u_t > 0, \quad 1 \leq s \leq t \leq n,$$

i.e. for any given network segment $(s-1, t)$ where $1 \leq s \leq t \leq n$, the multiplication $\underline{A}_s \cdots \underline{A}_{t-1}$ over the segement $(s-1, t-1)$ times u_t is strictly positive.

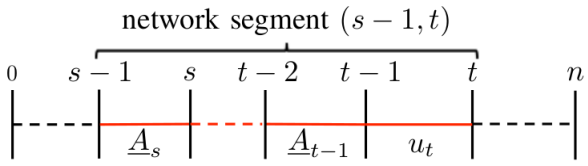

Figure 6.3: Illustrating C1: Line segment $(s-1, t)$ in an one feeder network with n nodes. $C1$ requires that for any such highlighted line segment in G the product of A over $(s-1, t-1)$ and u_t is greater than zero

6.1.3 Extension to Network Expansion Planning

A new proposition is introduced to extend this theorem for the network expansion problem.

Proposition 1. *If* $(r, x) \leq (r', x')$ *and* $C1$ *holds for* $(r', x', \overline{p}, \overline{q}, \underline{v})$*, then* $C1$ *also holds for* $(r, x, \overline{p}, \overline{q}, \underline{v})$

Three remarks can be drawn from this proposition. Firstly, Proposition 1 implies that the smaller the resistance and reactance is for the lines, the more likely $C1$ holds. As the resistance and reactance are anti-propotional to the maximal allowed current on a line (see (6.8) and (6.9)), network expansion benefits $C1$.

Secondly, it means that if $C1$ holds to begin with, i.e. for the initial parameters of the lines, it will also hold after the optimization due to the fact that existing lines are reinforeced only.

Finally, if $C1$ does not hold with the initial parameter of the lines, it may hold after performing the optimized network expansion and the SOCP becomes exact if $C2$ holds. To prove Proposition 1, the following Lemma is introduced. It is adapted from *Lemma 3* in [27] by focusing on the line parameters r and x rather than on power injection.

Lemma 1. *Given* $m \geq 1$ *and* $d \geq 1$*. Let* $\underline{A}_1 \cdots \underline{A}_{m-1}, A_1 \cdots A_{m-1} \in \mathbf{R}^{d \times d}$*,* $b_k^T \geq 0$*, and* $u_1, \ldots, u_m \in \mathbf{R}^d$ *satisfy*

- $\underline{A}_s \cdots \underline{A}_{t-1} u_t > 0$ *when* $1 \geq s \geq t \geq m$*;*
- *there exists* $\Delta u_k \in \mathbf{R}^d$*, with* $\Delta u_k \geq 0$ *and* $A_k - \underline{A}_k = (\underline{u}_k - u_k) b_k^T = \Delta u_k b_k^T$*, for* $k = 1, \ldots, m-1$

Then

$$A_s \cdots A_{t-1} u_t \geq \underline{A}_s \cdots \underline{A}_{t-1} u_t > 0 \tag{6.12}$$

when $1 \leq s \leq t \leq m$ *for any* $u_t > 0$*.*

Proof. (6.12) is proven by mathematical induction on the length of the segment $t - s$.

i) *Base Case*: When $t - s = 0$, one has $A_s \cdots A_{t-1} u_t = u_t \geq \underline{A}_s \cdots \underline{A}_{t-1} u_t > 0$. So, (6.12) holds.

ii) *Inductive Step*: Assume (6.12) holds when $t - s = 0, 1, \ldots, K\,(0 \leq K \leq m-2)$. When $t - s = K + 1$, one has

$$\begin{aligned} A_s \cdots A_k \underline{A}_{k+1} \cdots \underline{A}_{t-1} u_t &= A_s \cdots A_{k-1} \underline{A}_k \cdots \underline{A}_{t-1} u_t \\ &\quad + A_s \cdots A_{k-1}(A_k - \underline{A}_k)\underline{A}_{k+1} \cdots \underline{A}_{t-1} u_t \qquad (6.13) \\ &= \mathbf{A} u_t + A_s \cdots A_{k-1}(\underline{u}_k - u_k) b_k^T \underline{A}_{k+1} \cdots \underline{A}_{t-1} u_t \qquad (6.14) \end{aligned}$$

where $\mathbf{A} = A_s \cdots A_{k-1}\underline{A}_k \cdots \underline{A}_{t-1}$. (6.13) is obtained by adding and subtracting the term $A_s \cdots A_{k-1}\underline{A}_k \cdots \underline{A}_{t-1}u_t$. With $b_k^T \underline{A}_{k+1} \cdots \underline{A}_{t-1} u_t \in \mathbf{R}$, it follows for (6.14)

$$\begin{aligned} A_s \cdots A_k \underline{A}_{k+1} \cdots \underline{A}_{t-1} u_t &= \mathbf{A} u_t + (b_k^T \underline{A}_{k+1} \cdots \underline{A}_{t-1} u_t) A_s \cdots A_{k-1}(\underline{u}_k - u_k) \\ &= \mathbf{A} u_t + (b_k^T \underline{A}_{k+1} \cdots \underline{A}_{t-1} u_t) A_s \cdots A_{k-1}(\Delta u_k) \qquad (6.15) \end{aligned}$$

for $k = s, \ldots, t-1$. Since $b_k^T \geq 0$, $\underline{A}_{k+1} \cdots \underline{A}_{t-1} u_t > 0$. $\Delta u_k \geq 0$. According to induction hypothesis, $A_s \cdots A_{k-1} u_k > 0$ and since $\underline{u}_k \geq u_k$ it follows that the term $A_s \cdots A_{k-1}\Delta u_k \geq 0$. Hence,

$$A_s \cdots A_k \underline{A}_{k+1} \cdots \underline{A}_{t-1} u_t \geq A_s \cdots A_{k-1} \underline{A}_k \cdots \underline{A}_{t-1} u_t \qquad (6.16)$$

for $k = s, \ldots, t-1$. By substituting $k = t-1, \ldots, s$ in turn, one obtains

$$A_s \cdots A_{t-1} u_t \geq A_s \cdots A_{t-2} \underline{A}_{t-1} u_t \geq \cdots \geq \underline{A}_s \cdots \underline{A}_{t-1} u_t > 0, \qquad (6.17)$$

so (6.12) holds when $t - s = K + 1$.

According to i) and ii), (6.12) holds when $t - s = 0, \ldots, m-1$. This completes the proof of Lemma 1

□

With this lemma, the proof of Proposition 1 follows:

Proof. Let $\underline{A}'$ and $\underline{A}$ denote the matrices with respect to (r', x') and (r, x), respectively, i.e.

$$\underline{A}_i' \coloneqq I - \frac{2}{\underline{v}_i} u_i' \begin{pmatrix} \hat{P}_{ij}^+(\overline{p}) & \hat{Q}_{ij}^+(\overline{q}) \end{pmatrix} \quad \text{and} \quad \underline{A}_i \coloneqq I - \frac{2}{\underline{v}_i} u_i \begin{pmatrix} \hat{P}_{ij}^+(\overline{p}) & \hat{Q}_{ij}^+(\overline{q}) \end{pmatrix}$$

with $u_i' = \begin{pmatrix} r_{ij}' & x_{ij}' \end{pmatrix}^T$ and $u_i = \begin{pmatrix} r_{ij}' & x_{ij} \end{pmatrix}^T$ for any $(i,j) \in E$. For any edge (i,j) in G, one has

$$\begin{aligned} \underline{A}_i - \underline{A}_i' &= \frac{2}{\underline{v}_i} (u_i' - u_i) \begin{pmatrix} \hat{P}_{ij}^+ & \hat{Q}_{ij}^+ \end{pmatrix} \\ &= \Delta u_i \frac{2}{\underline{v}_i} \begin{pmatrix} \hat{P}_{ij}^+ & \hat{Q}_{ij}^+ \end{pmatrix} \\ &= \Delta u_i b_i^T \end{aligned}$$

where $b_i^T = \frac{2}{\underline{v}_i} \begin{pmatrix} \hat{P}_{ij}^+ & \hat{Q}_{ij}^+ \end{pmatrix} \geq 0$. When $(r,x) \leq (r',x')$, then

$$\Delta u_i = \begin{pmatrix} r_{ij}' - r_{ij} \\ x_{ij}' - x_{ij} \end{pmatrix} \geq 0$$

for any $(i,j) \in E$. If $C1$ holds for (r',x'), i.e. $\underline{A}_s' \cdots \underline{A}_{t-1}' u_t' > 0$ for any $l \in L$ and any s, t such that $1 \leq s \leq t \leq n_l$, then it follows from Lemma 1 that

$$\underline{A}_s \cdots \underline{A}_{t-1} u_t' \geq \overbrace{\underline{A}_s' \cdots \underline{A}_{t-1}' u_t' > 0}^{C1}$$

From (6.8) and (6.9) it follows that the ratio of r_{ij} and x_{ij}, $\frac{r_{ij}}{x_{ij}}$, for all $(i,j) \in E$ is constant, when performing network expansion. Thus, one can replac u_t' by u_t with $u_t' = n_t u_t$ with $n_t \geq 1$ and $n_t \in \mathbb{R}$ yielding

$$\underline{A}_s \cdots \underline{A}_{t-1} u_t > 0$$

for any $l \in L$ and any s, t such that $1 \leq s \leq t \leq n_l$. Hence, $C1$ holds also for (r,x), which completes the proof of Proposition 1. □

With Proposition 1 proven, Theorem 1 can be reformulated as follows

Theorem 2. *Assume that $C_g(s_0)$ is strictly increasing, that there exists $\overline{p}_i$ and $\overline{q}_i$ such that $S_i \subseteq \{s \in \mathbb{C} | Re(s) \leq \overline{p}_i, Im(s) \leq \overline{q}_i\}$ for $i \in N^+$, and there exists r_{ij} and x_{ij} such that $z_{ij} \subseteq \{z \in \mathbb{C} | Re(z) \leq r_{ij}, Im(z) \leq x_{ij}\}$ for $(i,j) \in E$. Then SOCP is exact if the following conditions hold:*

C1 $\underline{A}_{l_s} \cdots \underline{A}_{l_{t-1}} u_{l_t} > 0$ for any $l \in L$ and any s, t such that $1 \leq s \leq t \leq n_l$,

C2 every SOCP solution $w = (s, S, v, \ell, s_0)$ satisfies $s \in S_{volt}$, where $S_{volt} :=$ $\{s \in \mathbb{C}^n | \hat{v}(s) \leq v_i$ for $i \in N^+\}$

The interpretation of the theorem is similar to the one given in section 6.1.2 only with the extension of the line variables z. With the Proposition 1, it is made sure that the condition will hold considering smaller values of z, i.e. reinforced lines. The first condition $C1$ may be checked a priori but may improve with the optimization problem, see Proposition 1. The second condition $C2$ can only be check a posteriori as the solution for s is needed.

6.2 Relaxation of nonconvex current limit constraint

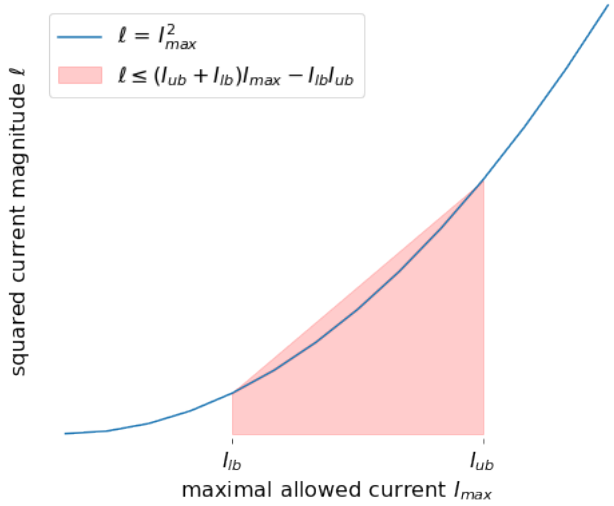

Figure 6.4: Convex relaxation of the nonconvex quadratic inequality current limit constraint

Another nonconvex constraint is the current limit constraint (1.6). To relax this constraint to a convex one, the overestimator from the *McCormick Envelopes* is used. McCormick Envelopes are a type of convex relaxation often used in bilinear NLP to describe the convex hull of a bilinear term of the form $z = xy$ where $x^L \leq x \leq x^U$ and $y^L \leq y \leq y^U$ [40]. They give a convex underestimator, (6.18)-6.19, and overestimator, (6.20)-(6.21), of the form

$$z \geq x^L y + x y^L - x^L y^L \tag{6.18}$$
$$z \geq x^U y + x y^U - x^U y^U \tag{6.19}$$

$$z \leq x^L y + x y^U - x^L y^U \tag{6.20}$$
$$z \leq x^U y + x y^L - x^U y^L \tag{6.21}$$

Let $z = I_{max}^2$ with $I_{lb} \leq I_{max} \leq I_{ub}$, then the McCormick overestimators, (6.20)-(6.21), give the same upperbound ($I_{lb} = x^L = y^L$ and $I_{ub} = x^U = y^U$) with

$$z \leq (I_{lb} + I_{ub})\, I_{max} - I_{lb} I_{ub}. \tag{6.22}$$

Using this upper bound as an upper bound on the current, the current limit constraint turns into

$$\ell \leq |I_{max}|^2 \qquad \Rightarrow \qquad \ell \leq (I_{lb} + I_{ub})\, I_{max} - I_{lb} I_{ub}, \tag{6.23}$$

which is illustrated in Fig. 6.4. It is not proven that this relaxation will be exact, i.e. $\ell \leq |I_{max}|^2$, but the following arguments give intuition, why this relaxation is valid and may result in an exact solution.

As the network planning problem, formulated in this thesis (1.1)-(1.8), considers a continuous expansion variables, in reality expansion of lines can be done in whole number only. Hence, the actual expansion will be the next largest number of the optimized value to ensure feasibility, which results in a greater margin between maximal allowed current and current flow.

Additionally, to provide security of supply if one line fails, medium voltage distribution networks are operated in an open ring structure. In the case if a line failure consumers are supplied from the other side of the ring. This in mind, assumptions are made in [6] and [2] that the flow over a line should not exceed 60 % of the thermal limit of the line when considering the so-called load case.

7 Numerical Study of Multiperiod OPF

In this chapter, three optimization problems considering a network expansion problem including storage systems are applied on for the 30 bus and 57 bus network, described in section 4.1. For each formulation, instances are created for time horizons $\mathcal{T} \in \{1, 2, \ldots, 7, 8, 10, 15\}$ with a timestep length $\boldsymbol{T_s} = 1$.

As the test network do not include any storage systems, a storage is added for any non-dispatchable volatile generator at the associated bus in the test networks. The storage data is shown in Table 7.1.

Table 7.1: Storage Data

Test network	Buses with storage	$\overline{e}$ MWh	$\overline{u_c}$ MW	$\overline{u_d}$ MW	$\boldsymbol{\eta_c}$ –	$\boldsymbol{\eta_d}$ –
30 bus network	11, 13	1.0	0.5	0.5	0.9	0.9
57 bus network	2, 6, 9	1.0	0.5	0.5	0.9	0.9

In the following, the formulations are presented and the results of the computational experiments are shown and discussed.

7.1 Formulations of Multiperiod OPF

The first formulation, **OPF**, represents the BFM with the original power flow equation, described in section 3.1, including the network expansion variables from section 3.2.2, and storage dynamics, i.e. relaxed complementary constraint (7.2), and state-of-charge over time (7.3) with periodic boundary conditions (7.4).

$$\textbf{OPF:} \quad \min_{\substack{p_g^t, q_g^t, v^t, \\ \ell^t, P^t, Q^t, I^{max}}} \quad \sum_{(i,k)\in E} c_{ik} I_{ik}^{max} + \sum_{t\in\mathcal{T}} \sum_{i\in N} C_g\left(p_{g,i}^t\right) \tag{7.1}$$

s.t. $(\forall t \in \mathcal{T})$

$(1.2) - (1.8)$

$$u_{c,i}^t \leq -\left(\frac{R_{c,i}^{max}}{R_{d,i}^{max}}\right) u_{d,i}^t + R_{c,i}^{max} \qquad \forall i \in S \qquad (7.2)$$

$$\boldsymbol{T_s}\left(\boldsymbol{\eta_{c,i}} u_{c,i}^t - \frac{u_{d,i}^t}{\boldsymbol{\eta_{d,i}}}\right) = e_i^{t+1} - e_i^t \qquad \forall i \in S \qquad (7.3)$$

$$e_i^{T+1} = e_i^0 \qquad \forall i \in S \qquad (7.4)$$

The second formulation, **crOPF**, contains the same constraints as in the OPF, but using the McCormick overestimator for the current limit constraint from section 6.2.

crOPF: $\min (7.1)$

s.t. $(\forall t \in \mathcal{T})$

$(1.2) - (1.5), (1.7), (1.8),$

$(7.2) - (7.4),$

$$\ell \leq (I_{lb} + I_{ub})\, I_{ik}^{max} - I_{lb} I_{ub}, \qquad \forall (i,j) \in E \qquad (7.5)$$

The third formulation, **SOC-crOPF**, is similar to crOPF, but uses the SOCP relaxation of the branch flow constraint, explained in section 6.1.

SOC-crOPF: $\min (7.1)$

s.t. $(\forall t \in \mathcal{T})$

$(1.2) - (1.5), (1.7), (1.8),$

$(7.2) - (7.4), (7.5)$

$$v_i \ell_{ij} \geq P_{ij}^2 + Q_{ij}^2, \qquad \forall\, (i,j) \in E \qquad (7.6)$$

7.2 Results

For all of the instances, a time limit of 3000 s and a primal-dual gap limit of 1 % is chosen. The primal-dual gap is defined by $gap\% = \frac{primal-dual}{primal} \times 100$.

7.2.1 30 Bus Case

Fig. 7.1 shows the computing time to find a solution and to prove global optimality with up to a primal-dual gap of 1 % for the OPF, crOPF, and SOC-crOPF formulation. Except for time horizons of length $\mathcal{T} = 8, 10, 15$ in the crOPF formulation, all instances are solved to global optimality in less than 1000 s.

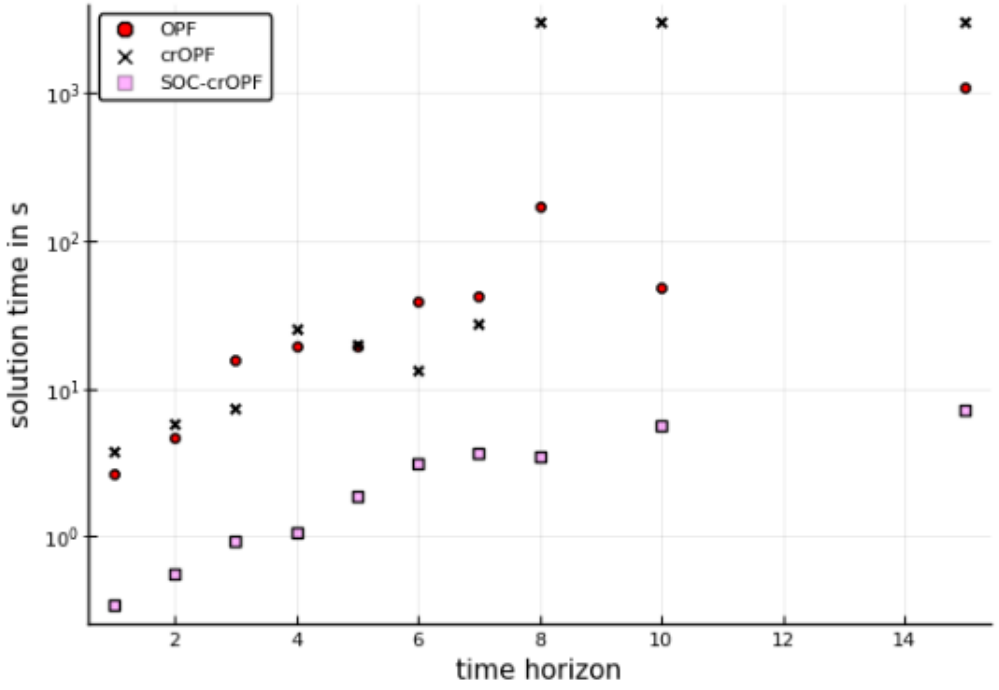

Figure 7.1: Computing time to find and prove global optimum (duality-gap < 1 %) using SCIP for **OPF** (circle), **crOPF** (cross), and **SOC-crOPF** (square) minimizing with respect to network expansion and generator use in a 30 bus test network including a storage systems at each fixed generator (two in total)

It is observed that solving the SOC-crOPF is faster with an order of ten compared to the other formulations. For time horizon $\mathcal{T} = 15$, it is even two order of ten faster. Furthermore, even though the crOPF has less nonconvex constraints, it is not solved any faster than the OPF. For longer time horizon it performs worse than OPF. The solution time to prove global optimality inclines exponentially with respect to the time horizon (linear incline in a semi-log plot).

The optimality gap between OPF and SOC-crOPF is zero for all considered time horizons, see Table 7.2, resulting in an exact solution for the SOC-crOPF.

Table 7.2: Objective values of 30 bus case

$\mathcal{T}$	OPF	crOPF	SOC-crOPF	gap = $\frac{\text{OPF}-\text{SOC-crOPF}}{\text{OPF}}$
1	7934.771266	7935.223386	7934.771061	10^{-8}
2	19553.11583	19553.11583	19553.115	10^{-8}
3	27906.44965	27906.44965	27906.44924	10^{-8}
4	38907.8019	38907.80200	38907.80151	10^{-8}
5	44822.49685	44822.49685	44822.49611	10^{-8}
6	57829.24982	57829.24982	57829.24906	10^{-8}
7	65543.34456	65543.34456	65543.34362	10^{-8}
8	77202.29642	96265.11381	77202.29541	10^{-8}
10	88471.76958	162762.7453	88471.76805	10^{-8}
15	139485.766	158852.0403	139485.7641	10^{-8}

7.2.2 57 Bus Case

Fig. 7.2 shows the computing time to solve the instances up to a primal-dual gap of 1 % for the OPF, crOPF, and SOC-crOPF for the 57 bus network with a time limit of 3000 s. The primal-dual gap is shown in Fig. 7.3.

Whenever the time limit is reached the gap is greater than 1 %. For time horizons $\mathcal{T} = 10, 15$ for OPF the gap is at 4 % and ∞, respectively, i.e. the OPF has not found a primal solution for $\mathcal{T} = 15$ yet. Considering the crOPF, for time horizons $\mathcal{T} = 4, 5, 6, 7, 8, 15$, the primal-dual gap is closed up to 3 % at most, for $\mathcal{T} = 4$ it is > 40 %.

In total, one can say, that the SOC-crOPF is solved significantly faster than the other two formulations. However, for time horizons $\mathcal{T} = 2, 3, 4$ the solution time rises for the OPF and SOC-crOPF, then drops for larger horizons again and differs compared to SOC-crOPF for the other time horizons more than two orders of tens.

There may be multiple reasons which cause this behaviour. On the one hand, this could be a statistical error and by adjusting these problem instances slightly, this deviation would disappear.

On the other hand, this behaviour could be systemically. A systemically reason could be the impact of the cost ratio between generation costs and expansion costs. The expansion costs do not depend on the length of the time horizon, whereas the generation costs rise as the time horizons get longer, which will be studied in the next section.

Table 7.3 shows the objective values for all formulation and the optimality gap between the OPF and SOC-crOPF. The optimality gap is in order of 10^{-4}. Thus, the SOC-crOPF gives a very good lower bound on the OPF problem. Only for time horizons $\mathcal{T} = 10, 15$, the gap is larger. As pointed out before, these are the time horizons for which SCIP could not a) close the primal-dual gap below 1 % and b) find a primal solution in the given time limit.

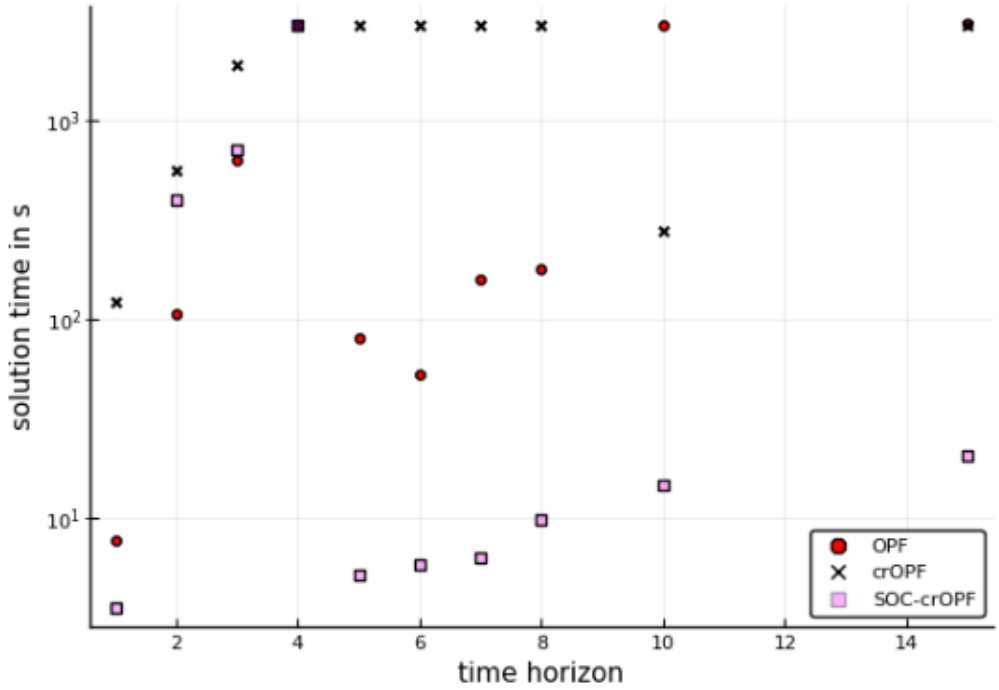

Figure 7.2: Computing time to find and prove global optimum (duality-gap < 1 %) using SCIP for **OPF** (circle), **crOPF** (cross), and **SOC-crOPF** (square) in a 57 bus test network including a storage systems at each fixed generator (three in total)

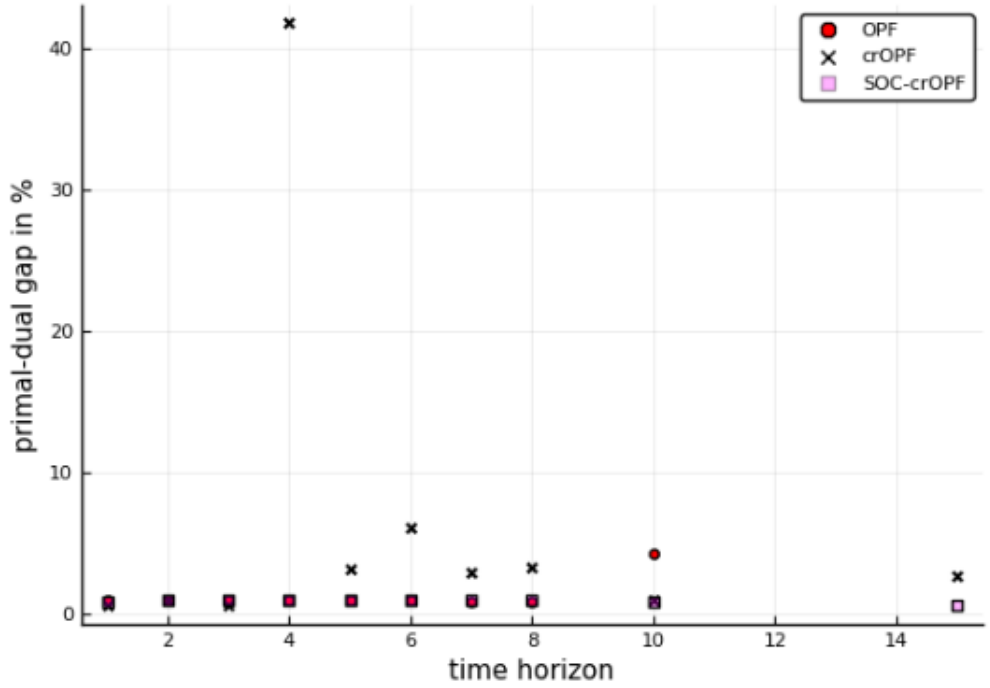

Figure 7.3: Primal-dual gap using SCIP for **OPF** (circle), **crOPF** (cross), and **SOC-crOPF** (square) in a 57 bus test network including a storage systems at each fixed generator (three in total)

Table 7.3: Objective values of 57 bus case

$\mathcal{T}$	OPF	crOPF	SOC-crOPF	gap $= \frac{\text{OPF}-\text{SOC-crOPF}}{\text{OPF}}$
1	16874.34936	16874.34936	16864.87517	5.61E-04
2	36824.45775	36824.45775	36806.31846	4.93E-04
3	53015.28495	53015.28495	52994.18688	3.98E-04
4	72098.50818	101193.77408	72074.69844	3.30E-04
5	85722.93405	87688.99377	85698.09105	2.90E-04
6	107134.34474	112667.72942	107107.36573	2.52E-04
7	122617.83226	125246.42911	122589.58825	2.30E-04
8	142434.53585	146116.67431	142404.95658	2.08E-04
10	175135.70817	169057.78201	169025.90442	3.49E-02
15	∞	265919.98139	260166.00327	–

7.3 Sensitivity study

In the following, a a sensitiviy study is performed on the cost weights of the expansion costs c_{ik}. The cost factor is chosen from the set $C = \{0.1, 1, 10, 100, 1000\}$. The sensitivity study is performed on the SOC-crOPF formulation for the 57 bus network. Again, a time limit of 3000 s and a primal-dual gap limit of 1 % is chosen for solving the problem with SCIP.

7.3.1 57 Bus Case

Fig.7.4 shows the computing time of the SOC-crOPF formulation for three time horizons, $\mathcal{T} = 2, 3, 4$, over the cost weights c_{ik} for the 57 bus network. Small cost weights resulting in solution times less than 10 seconds. For a cost weight of 1000 the primal-dual gap is closed to less than 1 % in under 10 s as well. For cost weights 10 and 100 the solution time increase in multiple orders of ten.

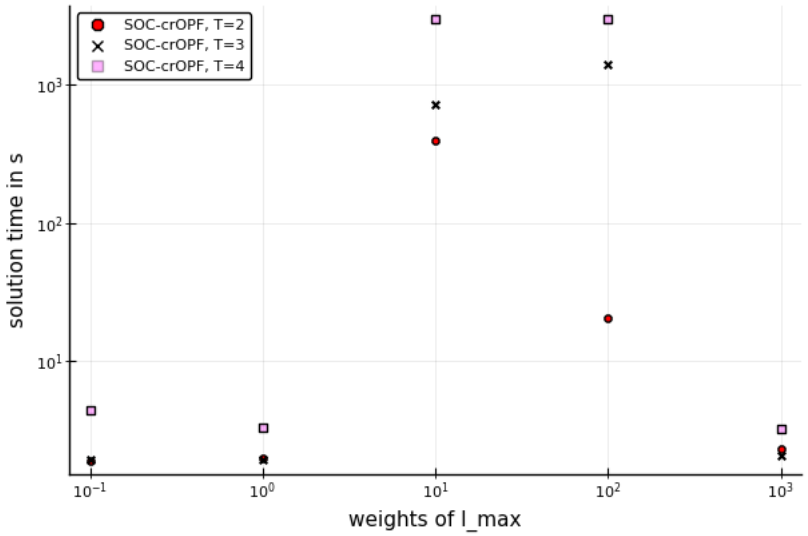

Figure 7.4: Computing time to find and prove global optimum (duality-gap < 1 %) in the SOC-crOPF with different weights of costs for three time horizons in the 57 bus network

Fig. 7.5 shows the change in variables for different weights of the expansion costs. On the left, to represent the change in variables for the maximal allowed current flow, i.e. the network expansion, all line capacities are summed. A exponential decline is observed over the increase of the attached cost weights. Whereas, on the right, the total generation costs are all most constant.

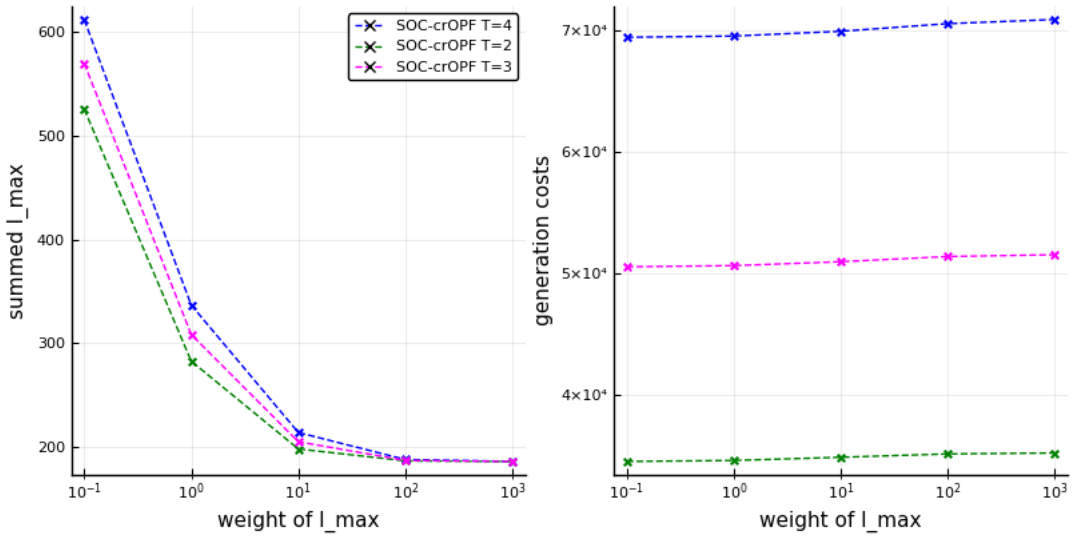

Figure 7.5: Change in variables for maximal allowed current flow (left) and power generation (right) over cost weights of network expansion for time horizons $\mathcal{T} = 2, 3, 4$ in the 57 bus network.

As the power injections directly depend on fixed generations and demand in the network, network expansion is used 1) to reinforce lines whenever overload or violation on voltage bounds are expected, and 2) to reduce losses over lines. Thus, the increase in costs for network expansion forces to find the minimal expansion needed for feasibility reasons. Whereas, the decrease in costs allows excessive network expansion to reduce losses in the system.

7.4 Conclusion

In this chapter, computational experiments are performed on the original multiperiod OPF and two similar formulation containing relaxations of nonconvex constraints, introduced in chapter 6. In particular through the SOC relaxation, a significant speed-up to find globally optimal solutions is obtaind. For the 30 bus network the relaxation resulted in an exact solution, while it provided a very good lower bound for the 57 bus network.

A sensitive study on the cost weights of the network expansion variable shows that 1) solution time might depend on the ratio of network expansion costs and generation costs, and 2) the impact of the weights of network expansion cost is much greater on the actual network expansion variable than on the power generation.

8 Résumé

8.1 Summary

The recent development of medium voltage distribution networks, in particular the incline of complexity through a number of flexibility options in these networks, motivates to investigate OPF formulations including these options to ensure a cost optimal system operation and planning. For instance, managing distributed RES and storage systems may play an increasing role in avoiding necessary network expansion. However, these components introduce a temporal coupling into the problem resulting in a multiperiod OPF.

As valid assumptions to solve a linearized OPF in transmission networks fail in distribution networks, a nonlinear formulation has to be considered. In this thesis, such a nonlinear multiperiod OPF problem includes storage systems and a continuous representation of network expansion and is presented in Section 1.2.

Network expansion is usually formulated in a MIP which is in general hard to solve. In this work, a continuous representation of the network expansion problem is provided by introducing continuous variables for technical parameters of the lines, i.e. maximal allowed current, resistance and reactance. This approach is validated successfully against a common mixed integer approach on a 30 and 57 bus network, resulting in an significant speed-up, see Chapter 5.

However, nonconvexities arise by the power flow equations as well as by the network expansion variables resulting again in a generally hard solvable optimization problem. Thus, convexifying the problem through relaxations of the nonconvexities is investigated. A new proposition is introduced and proven to extend earlier proposed sufficient conditions, see [27] and Chapter 7, to guarantee exactness of an SOCP relaxation of the branch flow constraint in radial networks including network expansion. Additionally, the McCormick overestimator is used to relax the current limit constraint.

These relaxations are then applied on the original proposed multiperiod OPF

and numerical experiments are performed on a 30 and 57 bus network in Chapter 7. In partiular, with the SOCP relaxation a massive speed-up in computing time is gained to find and prove global optimality. Further, the experiment show that the SOCP relaxation gives either an exact solution of the problem or a good lower bound on the solution.

Finally, a sensitive study on the cost weights of the network expansion variables is performed showing that the actual performed expansion depends strongly on the network expansion costs, whereas − as expected − almost no impact on the power generation is detected. Also, the weights of network expansion costs affect the computing time. But, further experiments are needed to verify if this is a statistical or systemically behaviour.

8.2 Future Research

This thesis constitutes an analysis of a continuous formulation of the network expansion planning problem. It motiviates a number of future research directions. Future research should conists of both further analysis of the nonconvexities in the problem and further numerical studies.

Even by introducing a SOCP relaxation of the branch flow constraint and the McCormick overestimator (see Chapter 6), the multiperiod OPF in this thesis still consists of quadratic equality constraints, e.g. the terms with $r\ell$ or $x\ell$ in the voltage differences between the buses (1.4), which are nonconvex.

To use the characteristic of convex problems, i.e. every local optimum is a global optimum, one should look into relaxing the problem further to obtain a convex problem. Additionally, it should be examined whether the sufficient conditions, presented in Chapter 6, are suitable for real network data.

The numerical studies performed in this thesis consider two small test networks and a single time series. To gain more knowledge about the behaviour of the problems, one should apply the discussed formulations on real network data as real distribution grids can contain around 250 buses [7], and on a variation of time series to investigate uncertainties in forecast and statistical behaviour of the problems. Furthermore, to use the potential of a multiperiod approach fully, longer time horizons should be taken into account.

These extensions − larger networks and longer time horizons − lead to a significant increase in the number of variables and constraints. In particular, reducing temporal complexity may result in a substantial improvement, possible

keywords are aggregation or clustering of time periods.

Another way to reduce variables in the problem would be to identify critical parts of the network a priori, e.g. by a power flow analysis [7], to define a subset of candidate lines which may be reinforced, followed by the actual optimization.

Moreover, there are a number of flexibility options which may be used to avoid network expansion and should be integrated into the problem formulation [31]. In this thesis, storage systems are already installed with a given capacity at non-dispatchable generators, but these may not be optimal. Hence, optimizing storage capacity and position may reduce necessary network expansion further.

Another flexibility options, which should be taken into account, is the curtailment of renewable energy sources through out the network. In the Germany for instance, annual curtailment of around 2 percentage of the possible power generation by renewable energy sources is allowed by law [41].

Bibliography

[1] J. Büchner, J. Katzfey, O. Floercken, A. Moser, H. Schuster, S. Dierkes, T. van Leeuwen, L. Verheggen, M. Uslar, and M. van Amelsvoort, "Moderne Verteilernetze fÃ¼r Deutschland (Verteilernetzstudie)," tech. rep., BMWi, 2014. Available online: https://www.bmwi.de/Redaktion/DE/Publikationen/Studien/verteilernetzstudie.pdf?__blob=publicationFile&v=5 (accessed on 21 November 2019).

[2] A. C. Agricola, B. Höflich, P. Richard, J. Völker, C. Rehtanz, G. M., B. Gwisdorf, J. Kays, T. Noll, J. Schwippe, A. Seack, J. Teuwsen, G. Brunekreeft, R. Meyer, and V. Liebert, "Ausbau- und Innovationsbedarf der Stromverteilnetze in Deutschland bis 2030 (kurz: dena-Verteilnetzstudie)," Endbericht, Deutsche Energie-Agentur GmbH (dena), 2012. https://www.dena.de/fileadmin/dena/Dokumente/Themen_und_Projekte/Energiesysteme/dena-Verteilnetzstudie/denaVNS_Ergebniszusammenfassung_PSG.pdf.

[3] Federal Ministry of Justice and Consumer Protection, "Law on Electricity and Gas Supply (Energiewirtschaftsgesetz - EnWG)," 2005. Available online: https://www.gesetze-im-internet.de/enwg_2005/BJNR197010005.html.

[4] J. A. Taylor, *Convex Optimization of Power Systems*. Cambridge University Press, 2015.

[5] D. K. Molzahn and I. A. Hiskens, "A Survey of Relaxations and Approximations of the Power Flow Equations," vol. 4, pp. 1–221, 01 2019.

[6] C. Rehtanz, M. Greve, U. Häger, Z. Hagemann, S. Kippelt, C. Kittl, M.-L. Kloubert, O. Pohl, F. Rewald, and C. Wagner, "Verteilnetzstudie für das Land Baden-Württemberg," tech. rep., ef.Ruhr GmbH, 2017.

[7] U. P. Müller, B. Schachler, W.-D. Bunke, J. Bartels, M. Glauer, C. Büttner, S. Günther, E. Kötter, I. Cußmann, L. Hülk, M. Scharf, T. Mossakowski, and J. Wendiggensen, "Netzebenenübergreifendes Planungsinstrument - zur Bestimmung des optimalen Netz- und Speicherausbaus in Deutschland - integriert in einer OpenEnergy-Plattform," Projektabschlussbericht, 2019. `https://openegoproject.wordpress.com/`.

[8] J. F. Franco, L. F. Ochoa, and R. Romero, "Ac opf for smart distribution networks: An efficient and robust quadratic approach," *IEEE Transactions on Smart Grid*, vol. 9, pp. 4613–4623, Sep. 2018.

[9] M. Farivar and S. H. Low, "Branch Flow Model: Relaxations and Convexification - Part I," *IEEE Transactions on Power Systems*, vol. 28, pp. 2554–2564, Aug 2013.

[10] R. A. Jabr, "Optimization of AC Transmission System Planning," *IEEE Transactions on Power Systems*, vol. 28, pp. 2779–2787, Aug 2013.

[11] J. F. Marley, D. K. Molzahn, and I. A. Hiskens, "Solving multiperiod OPF problems using an AC-QP algorithm initialized with an SOCP relaxation," *IEEE Transactions on Power Systems*, vol. 32, pp. 3538–3548, Sep. 2017.

[12] J. Carpentier, "Contribution a l'etude du dispatching economique," *Bulletin de la Societe Francoise de Electriciens*, vol. 8, no. 3, pp. 431–447, 1962.

[13] M. B. Cain, R. P. O'Neill, and A. Castillo, "History of optimal power flow and formulations," 2012.

[14] S. Frank, I. Steponavičė, and S. Rebennack, "Optimal power flow: a bibliographic survey I," *Energy Systems*, vol. 3, 09 2012.

[15] M. E. Baran and F. F. Wu, "Optimal capacitor placement on radial distribution systems," *IEEE Transactions on Power Delivery*, vol. 4, pp. 725–734, Jan 1989.

[16] C. Coffrin, H. L. Hijazi, and P. Van Hentenryck, "DistFlow Extensions for AC Transmission Systems," *arXiv e-prints*, p. arXiv:1506.04773, May 2015.

[17] A. Gopalakrishnan, A. U. Raghunathan, D. Nikovski, and L. T. Biegler, "Global optimization of multi-period optimal power flow," in *2013 American Control Conference*, pp. 1157–1164, June 2013.

[18] S. Boyd and L. Vandenberghe, *Convex Optimization*. Cambridge University Press, 7th ed., 2009.

[19] C. Coffrin, H. L. Hijazi, and P. Van Hentenryck, "The qc relaxation: A theoretical and computational study on optimal power flow," *IEEE Transactions on Power Systems*, vol. 31, pp. 3008–3018, July 2016.

[20] "Power Systems Test Case Archive." University of Washington Department of Electrical Engineering, Available: `http://labs.ece.uw.edu/pstca/` (accessed on 21 November 2019).

[21] L. Vandenberghe and M. S. Andersen, "Chordal graphs and semidefinite optimization," *Foundations and Trends in Optimization*, vol. 1, no. 4, pp. 241–433, 2015.

[22] R. A. Jabr, "Radial distribution load flow using conic programming," *IEEE Transactions on Power Systems*, vol. 21, pp. 1458–1459, Aug 2006.

[23] S. H. Low, "Convex relaxation of optimal power flow - part I: Formulation and Equivalence," *IEEE Transactions on Control of Network Systems*, vol. 1, pp. 177–189, June 2014.

[24] C. Bingane, M. F. Anjos, and S. Le Digabel, "Tight-and-cheap conic relaxation for the ac optimal power flow problem," *IEEE Transactions on Power Systems*, vol. 33, pp. 7181–7188, Nov 2018.

[25] S. H. Low, "Convex relaxation of optimal power flow - part II: Exactness," *IEEE Transactions on Control of Network Systems*, vol. 1, pp. 177–189, June 2014.

[26] S. Huang, Q. Wu, J. Wang, and H. Zhao, "A sufficient condition on convex relaxation of ac optimal power flow in distribution networks," *IEEE Transactions on Power Systems*, vol. 32, pp. 1359–1368, March 2017.

[27] L. Gan, N. Li, U. Topcu, and S. H. Low, "Exact convex relaxation of optimal power flow in radial networks," *IEEE Transactions on Automatic Control*, vol. 60, pp. 72–87, Jan 2015.

[28] L. H. Macedo, C. V. Montes, J. F. Franco, M. J. Rider, and R. Romero, "Milp branch flow model for concurrent ac multistage transmission expansion and reactive power planning with security constraints," *IET Generation, Transmission Distribution*, vol. 10, no. 12, pp. 3023–3032, 2016.

[29] I. B. Sperstad and M. Korpås, "Energy storage scheduling in distribution systems considering wind and photovoltaic generation uncertainties," *Energies*, vol. 12, no. 7, 2019.

[30] A. Maffei, D. Meola, G. Marafioti, G. Palmieri, L. Iannelli, G. Mathisen, E. Bjerkan, and L. Glielmo, "Optimal power flow model with energy storage, an extension towards large integration of renewable energy sources.," *IFAC Proceedings Volumes*, vol. 47, no. 3, pp. 9456 – 9461, 2014. 19th IFAC World Congress.

[31] "openBEA project." `https://openbeaproject.wordpress.com/`.

[32] R. L. Boylestad, *Introductory Circuit Analysis*. Upper Saddle River, NJ, USA: Pearson Prentice Hall Press, 11th ed., 2007.

[33] B. Kocuk, S. S. Dey, and X. A. Sun, "Inexactness of sdp relaxation and valid inequalities for optimal power flow," *IEEE Transactions on Power Systems*, vol. 31, pp. 642–651, Jan 2016.

[34] C. Coffrin, D. Gordon, and P. Scott, "Nesta, the NICTA energy system test case archive," *CoRR*, vol. abs/1411.0359, 2014.

[35] C. Coffrin, R. Bent, K. Sundar, Y. Ng, and M. Lubin, "Powermodels.jl: An open-source framework for exploring power flow formulations," in *2018 Power Systems Computation Conference (PSCC)*, pp. 1–8, June 2018.

[36] I. Dunning, J. Huchette, and M. Lubin, "Jump: A modeling language for mathematical optimization," *SIAM Review*, vol. 59, no. 2, pp. 295–320, 2017.

[37] A. Gleixner, M. Bastubbe, L. Eifler, T. Gally, G. Gamrath, R. L. Gottwald, G. Hendel, C. Hojny, T. Koch, M. E. Lübbecke, S. J. Maher, M. Miltenberger, B. Müller, M. E. Pfetsch, C. Puchert, D. Rehfeldt, F. Schlösser, C. Schubert, F. Serrano, Y. Shinano, J. M. Viernickel, M. Walter, F. Wegscheider, J. T. Witt, and J. Witzig, "The SCIP Optimization Suite 6.0," technical report, Optimization Online, July 2018.

[38] T. Achterberg, "Scip: solving constraint integer programs," *Mathematical Programming Computation*, vol. 1, pp. 1–41, Jul 2009.

[39] A. Wächter and L. T. Biegler, "On the implementation of an interior-point filter line-search algorithm for large-scale nonlinear programming," *Mathematical Programming*, vol. 106, pp. 25–57, Mar 2006.

[40] G. P. McCormick, "Computability of global solutions to factorable nonconvex programs: Part I — convex underestimating problems," *Mathematical Programming*, vol. 10, pp. 147–175, Dec 1976.

[41] Bundesministerium für Umwelt, Naturschutz und Reak- torsicherheit (Hrsg.), "Eckpunkte der EEG-Novelle sowie sonstige Neuerungen für erneuerbare Energien," 2011.